



A new series of bioactive $\text{Mo}^{(\text{V})}_2\text{O}_2\text{S}_2$ -based thiosemicarbazone complexes: Solution and DFT studies, and antifungal and antioxidant activities

Diana Cebotari ^{a,b}, Jordi Buils ^{c,d}, Olga Garbuz ^e, Greta Balan ^f, Jérôme Marrot ^a, Vincent Guérineau ^g, David Touboul ^g, Mohamed Haouas ^a, Mireia Segado-Centelles ^c, Carles Bo ^{c,*}, Aurelian Gulea ^{b,*}, Sébastien Floquet ^{a,*}

^a Institute Lavoisier de Versailles, CNRS UMR 8180, Univ. Versailles Saint Quentin en Yvelines, Université Paris-Saclay, 45 av. des Etats-Unis, 78035 Versailles cedex, France

^b State University of Moldova, 60 Alexei Mateevici str., MD-2009, Chisinau, Republic of Moldova

^c Institute of Chemical Research of Catalonia (ICIQ), The Barcelona Institute of Science and Technology, Av. Països Catalans 16, 43007 Tarragona, Spain

^d Departament de Química Física i Inorgànica, Universitat Rovira i Virgili, Tarragona, Spain

^e Institute of Zoology, 1 Academiei str., MD-2028, Chisinau, Republic of Moldova

^f State University of Medicine and Pharmacy "Nicolae Testemițanu", 165 Stefan cel Mare and Sfant Street, Chișinău MD-2004, Republic of Moldova

^g Université Paris-Saclay, CNRS, Institut de Chimie des Substances Naturelles, UPR 2301, 91198 Gif-sur-Yvette, France



ARTICLE INFO

Keywords:

Molybdenum
Cluster
Thiosemicarbazone
Coordination complex
Antioxidant
Antifungal

ABSTRACT

This paper deals with the synthesis, characterization, and studies of biological properties of a series of 5 coordination compounds based on binuclear core $[\text{Mo}^{(\text{V})}_2\text{O}_2\text{S}_2]^{2+}$ with thiosemicarbazones ligands bearing different substituents on the R^1 position of the ligand. The complexes are first studied using MALDI-TOF mass spectrometry and NMR spectroscopy to determine their structures in solution in relation to single-crystal X-Ray diffraction data. In a second part, the antifungal and antioxidative activities are explored and the high potential of these coordination compounds compared to the uncoordinated ligands is demonstrated for these properties. Finally, DFT calculation provides important support to the solution studies by identifying the most stable isomers in each $[\text{Mo}^{(\text{V})}_2\text{O}_2\text{S}_2]^{2+}/\text{Ligand}$ system, while the determination of HUMO and LUMO levels is performed to explain the antioxidative properties of these systems.

1. Introduction

Molybdenum (Mo) is present as trace element everywhere in nature, both in soils and in living organisms. Present in >50 enzymes, this element plays a crucial role in many biological processes, such as nitrogen assimilation by plants [1–3]. This implication in biology have prompted many authors to develop biomimetic Mo-based coordination complexes. In particular, many coordination complexes based on clusters $[\text{Mo}_2^{(\text{V})}\text{O}_2\text{E}_2]^{2+}$ (where E is an μ -oxo or a μ -sulfido bridging group) have been developed as biomimetic models for enzymes since the 1960s [4–6]. In these clusters, the two Mo(+V) are bound through a Mo–Mo bond, which renders these complexes diamagnetic and perfectly stable in air and in usual solvents but, surprisingly, the biological properties of such complexes have only recently been studied [7–11].

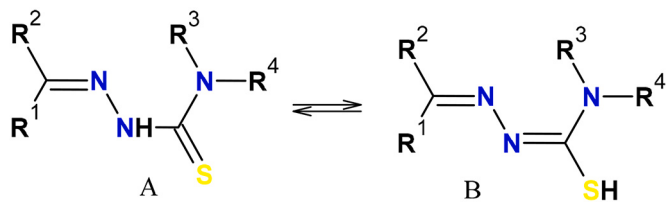
On the other hand, thiosemicarbazone ligands constitute a fascinating class of polydentate organic ligands of general formula $\text{R}^1\text{R}^2\text{C}=\text{N}-\text{NH-CS-NR}^3\text{R}^4$ (see Scheme 1) for which chemists can easily play on the nature of substituents R^1 , R^2 , R^3 and R^4 .

NH-CS-NR³R⁴ (see Scheme 1) for which chemists can easily play on the nature of substituents R^1 , R^2 , R^3 and R^4 .

This offers a huge panel of ligands capable of giving thousands of coordination complexes with transition metals [12–15], which have received considerable attention in many fields, such as biology and medicine [16–25]. Interestingly, despite the very large number of transition metal thiosemicarbazone complexes reported in the literature, molybdenum complexes are much rarer and often reported with Mo^(VI)-dioxo moieties such as $\text{MoO}_2(\text{L})$ -type complexes (where L is a tridentate thiosemicarbazone ligand), exhibiting antioxidant [26], antitumoral [27] and antibacterial [28] properties. Mo(+V) complexes are very scarce [29–32], which recently prompted us to develop a new family of $[\text{Mo}_2^{(\text{V})}\text{O}_2\text{S}_2]^{2+}$ -based thiosemicarbazones complexes with a wide panel of thiosemicarbazone ligands bearing various R^1 , R^2 , R^3 and R^4 substituents [33]. 14 new complexes based on $[\text{Mo}^{(\text{V})}_2\text{O}_2\text{S}_2]^{2+}$ have thus been synthesized, revealing unusual coordination modes of

* Corresponding authors.

E-mail addresses: cbo@iciq.cat (C. Bo), gulea@usm.md (A. Gulea), sebastien.floquet@uvsq.fr (S. Floquet).



Scheme 1. General representation of thiosemicarbazone ligand in its two forms (Thione A and Thiol B). The free ligands are usually in the A form, while the coordinated ligands are usually found in the deprotonated state of the B form.

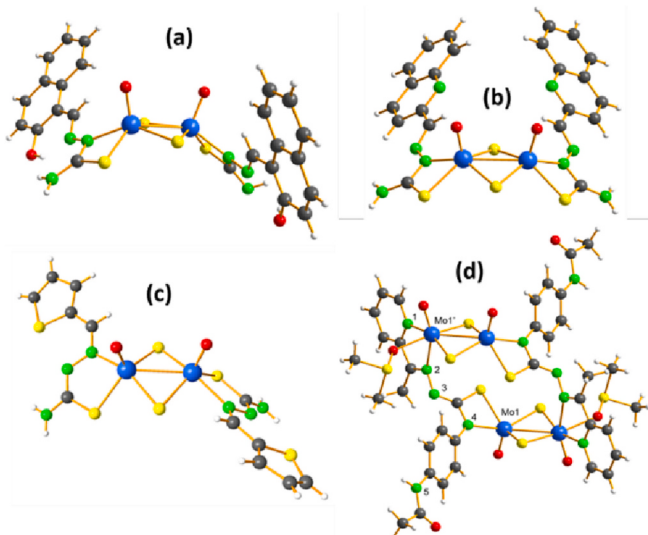


Fig. 1. Molecular structures of previous complexes a) $[\text{Mo}_2\text{O}_2\text{S}_2(\text{HL}^1)]_2$ (cis isomer), b) $[\text{Mo}_2\text{O}_2\text{S}_2(\text{L}^8)]_2$ (trans isomer), c) $[\text{Mo}_2\text{O}_2\text{S}_2(\text{L}^9)]_2$ (trans isomer) and d) $[\text{Mo}_2\text{O}_2\text{S}_2(\text{L}')_2(\text{DMSO})]_2$ (dimer), where HL^1 is defined for $\text{R}^1 = \text{H}$, $\text{R}^2 = \text{C}_{10}\text{H}_7\text{O}$, $\text{R}^3 = \text{H}$, $\text{R}^4 = \text{H}$, L^8 with $\text{R}^1 = \text{H}$, $\text{R}^2 = \text{C}_9\text{H}_6\text{N}$, $\text{R}^3 = \text{H}$, $\text{R}^4 = \text{H}$, L^9 with $\text{R}^1 = \text{H}$, $\text{R}^2 = \text{C}_4\text{H}_3\text{S}$, $\text{R}^3 = \text{H}$, $\text{R}^4 = \text{H}$, and L' with $\text{R}^1 = \text{CH}_3$, $\text{R}^2 = \text{C}_5\text{H}_4\text{N}$, $\text{R}^3 = \text{H}$, $\text{R}^4 = \text{C}_8\text{H}_8\text{NO}$, from Fuior et al. [33].

thiosemicarbazone ligands. Indeed, in 3d transition metal thiosemicarbazone complexes, 5-membered chelate rings are usually observed around the metal and the ligand are usually tridentate of types O,N,S or N,N,S. In the case of the coordination of $[\text{Mo}^{(\text{V})}_2\text{O}_2\text{S}_2]^{2+}$ the monoprotonated ligands act as bidentate N,S ligands with the cluster $[\text{Mo}^{(\text{V})}_2\text{O}_2\text{S}_2]^{2+}$ and 4-membered chelate rings are evidenced around Mo atoms by X-ray diffraction and by NMR studies in solutions, for giving essentially neutral complexes of stoichiometry cluster:ligand = 1:2. Some examples of structures obtained in our previous work are depicted in Fig. 1.

Surprisingly, studies of this new class of $[\text{Mo}^{(\text{V})}_2\text{O}_2\text{S}_2]^{2+}$ -thiosemicarbazone complexes showed that the imino group and the R^1

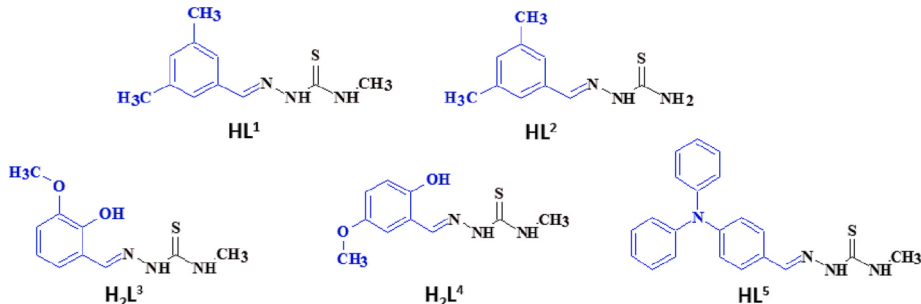
group never participate in the coordination with Mo, which contrasts with classical 3d transition metal complexes. Furthermore, we have shown that the nature of R^2 also plays an important role. Indeed, when $\text{R}^2 = \text{H}$, the formation of two isomers in solution in *cis* and *trans* configurations is systematically observed (see Fig. 1), while we identified up to 8 isomers in solution when $\text{R}^2 = \text{Me}$, due to a probable competition between the coordination of the imino group vs the coordination of the azomethinic N atom and thus between a 4- or 5-membered chelate ring on each Mo atom.

Very recently, the biological properties for these 14 new complexes were screened by Fuior et al. [34]. It was evidenced that the $\text{Mo}_2\text{O}_2\text{S}_2$ -based thiosemicarbazone complexes are of interest for biology and that the activity strongly depends on the nature of the R^1 group. When R^1 is a pyridine ring, a good activity of the complexes as antifungal is measured, while when R^1 is a phenol the antitumoral properties are enhanced. It is worth noting that for antifungal activity a good activity against *Cryptococcus neoformans* is measured for all complexes, while the activity against *Candida albicans* appears good only for complexes bearing pyridine derivatives. Finally, all complexes exhibit antioxidant properties better than TROLOX but the origin of the process was not established. Besides, the formation of mixtures of isomers constitutes a severe drawback for the interpretation of results in biology and ligands alone were only partially measured. The present study aims to address the issues evidenced by Fuior et al. with this new class of $\text{Mo}_2\text{O}_2\text{S}_2$ -based thiosemicarbazone complexes [33,34]:

- Controlling the formation of mixtures of isomers by introducing steric constraints.
- Changing the nature of R^1 group by a non-coordinative group to evaluate the impact on antifungal activity.
- Understanding the origin of the antioxidative properties, ligand, or molybdc cluster.

To address these issues, we synthesized 5 new ligands and the corresponding $[\text{Mo}^{(\text{V})}_2\text{O}_2\text{S}_2]^{2+}$ complexes. To limit the formation of isomers, the substituents $\text{R}^4 = \text{Me}$ or H , $\text{R}^3 = \text{H}$, and $\text{R}^2 = \text{H}$ were fixed, whereas we varied the nature of aldehyde in R^1 . Intuitively, if we want to favour the formation of a single isomer, we can for example introduce steric constraints between ligands. Besides, since R^1 has been shown to be not involved in coordination with Mo centres, we don't necessarily need a coordinating group present in R^1 . Consequently, we introduced in R^1 position a dimethylbenzene group for ligands HL^1 and HL^2 , 3- or 5-methoxy-salicylaldehyde for H_2L^3 and H_2L^4 , and the bulky substituent diphenylamine-benzaldehyde for ligand HL^5 (see Scheme 2). Each of them thus displays bulkier R^1 group than those used in our previous works in the hope of preventing isomers formation upon complexation with $[\text{Mo}^{(\text{V})}_2\text{O}_2\text{S}_2]^{2+}$. Furthermore, the ligands HL^1 and HL^2 possess a non-coordinative group as R^1 , which will permit to complete our previous studies, notably against fungi.

In this paper, a special attention is paid to combining NMR experimental and DFT studies to assess the effect of the variation of R^1 on the number of species formed in solution, so to better understand the



Scheme 2. Drawing of the ligands used in this study.

Table 1
Crystallographic data for $[\text{Mo}_2\text{O}_2\text{S}_2(\text{HL}^3)_2]\cdot2\text{DMSO}$ complex.

| Complex | $[\text{Mo}_2\text{O}_2\text{S}_2(\text{HL}^3)_2]\cdot2\text{DMSO}$ |
|--|---|
| Formula | $\text{C}_{24}\text{H}_{36}\text{Mo}_2\text{N}_6\text{O}_8\text{S}_6$ |
| M (g mol ⁻¹) | 920.83 |
| Crystal system | Triclinic |
| Space group | $\overline{\text{P}}\overline{\text{T}}$ |
| T (K) | 220 |
| Crystal | Yellow Parallelepiped |
| a (Å) | 9.8232(3) |
| b (Å) | 12.7500(4) |
| c (Å) | 14.6369(5) |
| α (°) | 93.020(2) |
| β (°) | 101.021(2) |
| γ (°) | 94.990(2) |
| V (Å ³) | 1788.07(10) |
| Z | 2 |
| D _{calc} (g cm ⁻³) | 1.710 |
| Crystal size (mm) | 0.28 × 0.18 × 0.10 mm |
| F(000) | 932 |
| $\mu(\text{Mo-K}\alpha)/\text{\AA}$ | 0.71073 |
| Reflections collected | 70,946 |
| Independent reflections ($I > 2\sigma(I)$) | 8345 |
| Parameters | 425 |
| $\Delta(\rho)$ (e Å ⁻³) | 1.22 and -0.80 |
| Goodness of fit | 1.05 |
| R ₁ ^a | 0.0307 (0.0443) ^b |
| wR ₂ ^a | 0.0692 (0.0771) ^b |

^a $R = \sum ||F_0| - |F_c|| / \sum |F_0|$, wR₂ = [$\sum w(F_0^2 - F_c^2)^2 / \sum w(F_0^2)^2$]^{1/2}; [F₀ > 4σ(F₀)].

^b Based on all data.

preferential formation of *cis* or *trans* isomers. The biological activity as antifungal and antioxidant is evaluated both for ligands and complexes, notably to evidence some selective properties. DFT calculations were performed on the ligands and *cis* and *trans* isomers of the complexes with the aim to determine the electronic levels and the nature of the frontier orbitals in the ligands and the complexes and to better understand the antioxidant activities of the complexes.

2. Experimental section

2.1. Materials and methods

Fourier Transform Infrared (FT-IR) spectra were recorded on a 6700 FT-IR Nicolet spectrophotometer, using diamond ATR technique. **Elemental analyses** were performed by Biocis laboratory, University Paris-Saclay (www.biocis.universite-paris-saclay.fr), Châtenay-Malabry, France. **EDX** measurements were performed on a JEOL JSM 5800LV apparatus.

Electrospray Ionization Mass Spectrometry (ESI-MS) spectra were collected for ligands by using a Q-TOF instrument supplied by WATERS. Samples were solubilized in CH₃CN at a concentration of 10⁻⁴ M. **MALDI-TOF mass Spectrometry**. MALDI-TOF spectra were recorded on a MALDI-TOF/TOF UltraflexXtreme mass spectrometer (Bruker Daltonics, Bremen) in reflector or linear positive ion mode as previously described [33].

Nuclear magnetic resonance (NMR) ¹H and ¹³C NMR spectra were measured in DMSO-*d*₆ deuterated solvent at 298 K on Bruker Avance 300 MHz spectrometer with 5 mm BBI probe head at 9.4 T. Chemical shifts are reported relative to 1% Me₄Si in CDCl₃. Simulation of NMR spectra were performed by using DMFIT software (free access through the link <https://cemhti.cnrs-orleans.fr/dmfit/>).

XRD analysis. Yellow-orange crystals of $[\text{Mo}_2\text{O}_2\text{S}_2(\text{HL}^3)_2]$ were obtained by recrystallization from DMSO solutions. The diffraction data were collected on a Bruker Apex Duo diffractometer with MoKα radiation ($\lambda = 0.71073$ Å) at 200 K. Crystals were glued in paratone oil to prevent any loss of crystallization solvents. An empirical absorption correction was applied using the SADABS program [35]. Structures were

solved by direct methods and refined by full-matrix least-squares treatment against | F |² in anisotropic approximation with SHELX 2014/7 set [36] using ShelXL program [37]. Further details about the crystal structure determinations may be obtained free of charge from the Cambridge Crystallographic Data Centre via www.ccdc.cam.ac.uk/data_request/cif on quoting the depository numbers CCDC-2191589. Crystallographic data are given in Table 1.

Computational details. The molecular geometry of all the complexes were fully optimized using a Density Functional Theory (DFT) method implemented in the Amsterdam Density Functional package [38] using the Slater TZP basis set from AMS library. We used the Becke and Perdew exchange-correlation functional (BP86) [39,40], together with the dispersion correction D3 from Grimme [41]. Relativistic corrections are included by the scalar Zero Order Regular Approximation (ZORA) [42]. Water solvation effects were considered employing the continuous Conductor like Screening Model (COSMO) [43] using the Klamt atomic radii. Analytical vibrational frequencies were computed for the stationary points to check their nature as minima in the energy surface. NMR chemical shifts were computed, using same functional and basis set as for geometry optimizations, and some values with TZ2P basis set.

A dataset collection of the computational results is available in the ioChem-BD repository and can be accessed via the following link: <https://doi.org/10.19061/iochem-bd-1-264>.

2.2. Protocols of biological tests

Antifungal activity tests were performed as described [34]. For minimum inhibitory concentration (MIC) assays a stock solution (10 mg/mL) of each test compound was prepared in dimethylsulfoxide (DMSO). This stock solution was then diluted in liquid RPMI (Roswell Park Memorial Institute) 1640 medium with both L-glutamine and 0.165 M MOPS buffer. The next dilutions were made using 2% of peptone bullion. The thermostating time depends on the generation time (multiplication time) of the microorganisms. The generation time for *Candida* spp. is about 160–180 min and up to 5 h for *Cryptococcus* spp. Visible growth on plates is possible for *Candida* spp. over 48 h and for *Cryptococcus* spp. over 72 h. The (MICs) were assessed visually after the corresponding incubation period and were taken as the lowest sample concentration at which there was no (or virtually) growth. For the minimum fungicidal concentrations (MFC) determination, 10 μL aliquots from each well that showed no growth of microorganism were plated on Mueller-Hinton Agar or Sabouraud Dextrose Agar and incubated at 37 °C for 48 h (*Candida* spp.), and 72 h (*Cryptococcus* spp.). The lowest concentration that yielded no growth after subculturing was taken as the MFC. Nystatin was used as the standard antifungal drug. All the experiments were carried out in triplicates.

In vitro antioxidant tests were performed by spectrophotometric method, where to solutions of specifically coloured free radicals (ABTS radical cation) is added to the experimental substance in different concentrations followed by absorbance measurements [34].

2.3. Chemicals and syntheses

The sulphurated precursor K_{1.5}(NMe₄)_{0.5}[I₂Mo₁₀O₁₀S₁₀(OH)₁₀(H₂O)₅]•20H₂O, denoted hereafter Mo₁₀, was prepared as described in the literature [44] and characterized by routine methods (FT-IR and TGA). Starting chemicals were purchased from Aldrich, Alfa Aesar or Acros companies and used without further purification.

2.3.1. Syntheses of ligands

Thiosemicarbazone ligands HL^{1, 2, 5} and H₂L^{3, 4} were synthesized by condensing aromatic aldehydes with thiosemicarbazide or methyl-thiosemicarbazide in a molar ratio of 1:1 in methanol or ethanol under reflux for 4 h in the presence of a few drops of acetic acid as a catalyst, as commonly described in literature [22,24,28,33,45]. The

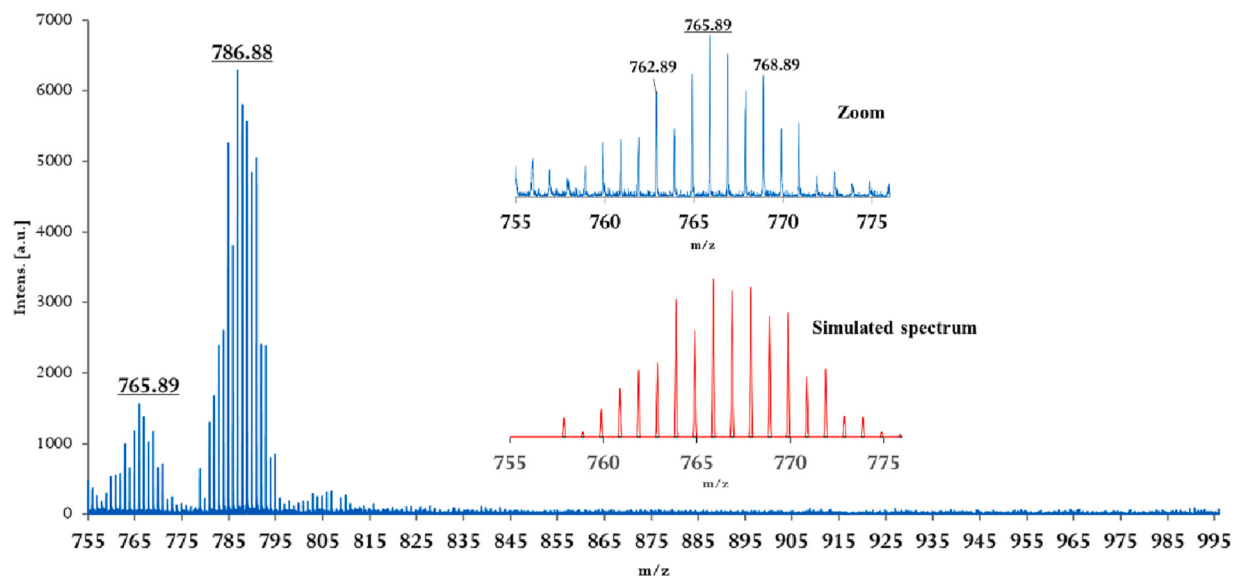


Fig. 2. MALDI-TOF mass spectrum of the compound $[\text{Mo}_2\text{O}_2\text{S}_2(\text{HL}^3)_2]$. The simulated spectrum is obtained with IsoPro3 freeware.

Table 2
MALDI-TOF data obtained for the complexes $[\text{Mo}_2\text{O}_2\text{S}_2(\text{H}_n\text{L}^{1-5})_2]$.

| Product | Exp. m/z | Assignment | Calc. m/z |
|--|---------------|--|----------------|
| $[\text{Mo}_2\text{O}_2\text{S}_2(\text{L}^1)_2]$ | 729.9 | $[\text{Mo}_2\text{O}_2\text{S}_2(\text{C}_{11}\text{H}_{14}\text{N}_3\text{S}_2) + \text{H}]^+$ | 729.6 |
| | 751.9 | $[\text{Mo}_2\text{O}_2\text{S}_2(\text{C}_{11}\text{H}_{14}\text{N}_3\text{S}_2) + \text{Na}]^+$ | 751.6 |
| $[\text{Mo}_2\text{O}_2\text{S}_2(\text{L}^2)_2]$ | 701.9 | $[\text{Mo}_2\text{O}_2\text{S}_2(\text{C}_{10}\text{H}_{12}\text{N}_3\text{S}_2) + \text{H}]^+$ | 701.6 |
| | 723.9 | $[\text{Mo}_2\text{O}_2\text{S}_2(\text{C}_{10}\text{H}_{12}\text{N}_3\text{S}_2) + \text{Na}]^+$ | 723.6 |
| $[\text{Mo}_2\text{O}_2\text{S}_2(\text{HL}^3)_2]$ | 765.8 | $[\text{Mo}_2\text{O}_2\text{S}_2(\text{C}_{10}\text{H}_{12}\text{N}_3\text{SO}_2)_2 + \text{H}]^+$ | 765.6 |
| | 787.8 | $[\text{Mo}_2\text{O}_2\text{S}_2(\text{C}_{10}\text{H}_{12}\text{N}_3\text{SO}_2)_2 + \text{Na}]^+$ | 787.6 |
| $[\text{Mo}_2\text{O}_2\text{S}_2(\text{HL}^4)_2]$ | 765.8 | $[\text{Mo}_2\text{O}_2\text{S}_2(\text{C}_{10}\text{H}_{12}\text{N}_3\text{SO}_2)_2 + \text{H}]^+$ | 765.6 |
| | 787.8 | $[\text{Mo}_2\text{O}_2\text{S}_2(\text{C}_{10}\text{H}_{12}\text{N}_3\text{SO}_2)_2 + \text{Na}]^+$ | 787.6 |
| $[\text{Mo}_2\text{O}_2\text{S}_2(\text{L}^5)_2]$ | 1007.9 | $[\text{Mo}_2\text{O}_2\text{S}_2(\text{C}_{21}\text{H}_{19}\text{N}_4\text{S})_2 + \text{H}]^+$ | 1007.9 |
| | 1029.9 | $[\text{Mo}_2\text{O}_2\text{S}_2(\text{C}_{21}\text{H}_{19}\text{N}_4\text{S})_2 + \text{Na}]^+$ | 1029.9 |

final reaction products are solid. They are isolated by filtration and washed with ethanol or methanol, dried under vacuum and characterized by FT-IR, ESI-MS, and ^1H and ^{13}C NMR spectroscopy. The ligands are all insoluble in water. However, they possess higher solubility in polar solvents, such as dimethylformamide (DMF), dimethylsulfoxide (DMSO), and acetonitrile (MeCN).

4-Methyl-3-thiosemicarbazone of 3,5-dimethylbenzaldehyde (HL^1). White powder (yield = 74%). FT-IR/cm $^{-1}$, (Diamond ATR): 3294 (m, sh.); 3115 (w); 2980 (w); 1591 (s); 1544 (m, sh.); 1515 (w, sh.); 1424 (s); 1371 (s); 1292 (m); 1242 (w); 1162 (s); 1087 (m); 1036 (m); 957 (m); 941 (vs); 900 (s); 845 (m); 802 (s); 706 (s); 685 (m); 656 (s); 617 (vs); 505 (vs); 448 (s). ^1H NMR: δ ppm (300 MHz/DMSO- d_6): 11.43 (s, 1H); 8.45 (m, 1H); 7.98 (s, 1H); 7.39 (s, 2H); 7.03 (s, 1H); 3.02 (d, 3H); 2.28 (s, 6H). ^{13}C NMR: δ ppm (300 MHz/DMSO- d_6): 177.6; 142.06; 137.72; 134.06; 131.26; 124.90; 30.81; 20.76. ESI: m/z Calc. (found) 222.3 (222.1) for molecular ion $[\text{M} + \text{H}]^+$.

Thiosemicarbazone of 3,5-dimethylbenzaldehyde (HL^2). White powder (yield = 79%). FT-IR/cm $^{-1}$, (Diamond ATR): 3392 (w); 3248 (m); 3155 (m); 3025 (s); 2913 (s); 1617 (s); 1599 (w); 1530 (vw); 1458 (s); 1385 (vs); 1364 (s); 1301 (m); 1216 (s, br.); 1175 (s); 1162 (s); 1096 (m); 1059 (s); 996 (vs); 946 (w); 849 (w); 834 (w); 713 (s); 688 (w); 621 (m); 563 (m, br.); 538 (s); 469 (s); 426 (s). ^1H NMR: δ ppm (300 MHz/DMSO- d_6): 11.30 (s, 1H); 8.20 (s, 1H); 7.96 (s, 2H); 7.39 (s, 2H); 7.00 (s, 1H); 2.26 (s, 6H). ^{13}C NMR: δ ppm (300 MHz/DMSO- d_6): 177.78; 142.50; 137.70; 133.98; 131.32; 125.03; 20.72. ESI: m/z Calc. (found) 208.3 (208.0) for molecular ion $[\text{M} + \text{H}]^+$.

4-Methyl-3-thiosemicarbazone of 2-hydroxy-3-methoxybenzan-

dehyde (H_2L^3). White powder (yield = 96%). FT-IR/cm $^{-1}$, (Diamond ATR): 3338 (s); 3305 (w, sh.); 1551 (w, sh.); 1527 (w, sh.); 1479 (w); 1447 (w); 1387 (vs); 1360 (s); 1331 (s); 1268 (w, br.); 1216 (w); 1186 (s); 1166 (s); 1108 (s); 1066 (w); 931 (m); 882 (vs); 831 (vs); 807 (m); 785 (m); 755 (s); 736 (m); 660 (s); 642 (s); 610 (s); 570 (s); 536 (m); 523 (m); 479 (vs); 403 (m). ^1H RMN: δ ppm (300 MHz/DMSO- d_6): 11.44 (s, 1H); 9.19 (s, 1H); 8.40 (q, 1H); 8.38 (s, 1H); 7.55 (d, 1H); 6.95 (d, 1H); 6.78 (t, 1H); 3.80 (s, 3H); 3.00 (d, 3H). ^{13}C RMN: δ ppm (300 MHz/DMSO- d_6): 177.49; 147.89; 145.83; 138.76; 120.87; 118.88; 117.99; 112.65; 55.86; 30.80. ESI: m/z Calc. (found) 240.3 (240.0) for molecular ion $[\text{M} + \text{H}]^+$.

4-Methyl-3-thiosemicarbazone of 2-hydroxy-5-methoxybenzaldehyde (H_2L^4). White powder (yield = 76%). FT-IR/cm $^{-1}$, (Diamond ATR): 3377 (vw, sh.); 3247 (vw, br.); 3012 (m); 2934 (m.); 2832 (s); 1621 (s); 1610 (s); 1578 (s); 1552 (vw, br.); 1518 (w); 1496 (m, br.); 1385 (s); 1369 (s); 1330 (vw, br.); 1262 (vw); 1239 (m); 1189 (m); 1167 (m); 1116 (s); 1089 (m); 1024 (w); 956 (s); 942 (s); 849 (s); 832 (m); 780 (m); 726 (s); 670 (s); 634 (vs); 609 (s); 571 (s); 526 (s); 498 (s); 469 (s). ^1H RMN: δ ppm (300 MHz/DMSO- d_6): 11.42 (s, 1H); 9.47 (s, 1H); 8.44 (q, 1H); 8.33 (s, 1H); 7.48 (d, 1H); 6.82 (d, 1H); 6.79 (s, 1H); 3.72 (s, 3H); 3.01 (d, 3H). ^{13}C RMN: δ ppm (300 MHz/DMSO- d_6): 177.27; 152.20; 150.46; 138.51; 120.77; 117.49; 116.72; 109.97; 55.59; 30.75. ESI: m/z Calc. (found) 240.3 (240.0) for molecular ion $[\text{M} + \text{H}]^+$.

4-Methyl-3-thiosemicarbazone of 4-(*N,N*-diphenylamino)benzaldehyde (HL^5). Yellow powder (yield = 89%). FT-IR/cm $^{-1}$, (Diamond ATR): 3370 (s); 3145 (m); 2995 (s); 1586 (vw); 1548 (w); 1505 (m); 1486 (vw); 1448 (vs); 1419 (s); 1382 (s); 1337 (s); 1320 (m); 1292 (m); 1265 (vw); 1165 (m); 1147 (s); 1079 (s); 1036 (s); 995 (vs); 932 (s); 904 (vs); 830 (s); 782 (s); 764 (m); 755 (m); 726 (s); 709 (s); 700 (s); 692 (m); 632 (s); 621 (s); 615 (s); 606 (s); 579 (s, br.); 537 (s); 527 (m); 511 (s); 492 (s); 446 (s); 524 (s); 407 (m). ^1H NMR: δ ppm (300 MHz/DMSO- d_6): 11.40 (s, 1H); 9.39 (m, 1H); 7.96 (s, 1H); 7.65 (d, 2H); 7.33 (t, 4H); 7.11 (d, 2H); 7.06 (d, 4H); 6.91 (d, 2H); 2.99 (d, 3H). ^{13}C NMR: δ ppm (300 MHz/DMSO- d_6): 177.36; 148.60; 146.54; 141.38; 129.67; 128.36; 127.65; 124.74; 123.85; 121.49; 30.75. ESI: m/z Calc. (found) 361.4 (361.1) for molecular ion $[\text{M} + \text{H}]^+$.

Fig. S1 depicts the FT-IR spectra of ligands. ESI-MS spectra of ligands are given in Figs. S2-S6 (Supporting Information), while ^{13}C and ^1H NMR data and spectra can be found in Table S1 and in Figs. S12-S20.

2.3.2. Syntheses of $[\text{Mo}^{(V)}\text{O}_2\text{S}_2]^{2+}$ complexes

The solid thiosemicarbazone ligand $\text{HL}^{1, 2, 5}$ or $\text{H}_2\text{L}^{3, 4}$ (0.833 mmol)

Table 3Selected bond lengths around Mo atoms (\AA) in $[\text{Mo}_2\text{O}_2\text{S}_2(\text{HL}^3)_2] \cdot 2\text{DMSO}$ crystal structure and in molecular structures optimized by DFT calculation.

| Complexes | Mo-Mo | Mo = O | Mo-N | Mo-S (bridges) | Mo-S (Ligand) | C-S | (N)N=C(S) |
|---|-------|----------------|----------------|----------------------------------|------------------|----------------|----------------|
| <i>Experimental XRD structure</i> | | | | | | | |
| <i>Trans</i> - $[\text{Mo}_2\text{O}_2\text{S}_2(\text{HL}^3)_2]$ | 2.831 | 1.678 1.675 | 2.135 2.137 | 2.341 2.303 2.334 | 2.460 2.441 | 1.745 1.745 | 1.330 1.338 |
| <i>Optimized structures by DFT</i> | | | | | | | |
| <i>cis</i> - $[\text{Mo}_2\text{O}_2\text{S}_2(\text{L}^1)_2]$ | 2.852 | 1.713 1.714 | 2.162 2.167 | 2.354 2.332 2.344 2.322 | 2.492 2.491 | 1.752 1.756 | 1.349 1.345 |
| <i>trans</i> - $[\text{Mo}_2\text{O}_2\text{S}_2(\text{L}^1)_2]$ | 2.852 | 1.715 1.715 | 2.150 2.150 | 2.365 2.364 2.322 | 2.486 2.486 | 1.752 1.752 | 1.345 1.345 |
| <i>cis</i> - $[\text{Mo}_2\text{O}_2\text{S}_2(\text{L}^2)_2]$ | 2.873 | 1.713 1.714 | 2.154 2.159 | 2.324 2.343 2.348 2.364 | 2.501 2.503 | 1.744 1.746 | 1.343 1.341 |
| <i>trans</i> - $[\text{Mo}_2\text{O}_2\text{S}_2(\text{L}^2)_2]$ | 2.849 | 1.714 1.714 | 2.157 2.158 | 2.320 2.364 2.321 2.353 | 2.487 2.484 | 1.751 1.751 | 1.338 1.338 |
| <i>cis</i> - $[\text{Mo}_2\text{O}_2\text{S}_2(\text{HL}^3)_2]$ | 2.867 | 1.713 1.714 | 2.161 2.163 | 2.323 2.339 2.345 2.369 | 2.501 2.515 | 1.749 1.744 | 1.347 1.351 |
| <i>trans</i> - $[\text{Mo}_2\text{O}_2\text{S}_2(\text{HL}^3)_2]$ | 2.837 | 1.718 1.720 | 2.185 2.161 | 2.322 2.325 2.358 2.335 | 2.462 2.494 | 1.752 1.767 | 1.348 1.339 |
| <i>cis</i> - $[\text{Mo}_2\text{O}_2\text{S}_2(\text{HL}^4)_2]$ | 2.866 | 1.713 1.714 | 2.160 2.159 | 2.328 2.347 2.351 2.357 | 2.505 2.507 | 1.748 1.747 | 1.349 1.349 |
| <i>trans</i> - $[\text{Mo}_2\text{O}_2\text{S}_2(\text{HL}^4)_2]$ | 2.839 | 1.718 1.719 | 2.161 2.167 | 2.323 2.370 2.323 2.334 | 2.494 2.486 | 1.755 1.752 | 1.346 1.348 |
| <i>cis</i> - $[\text{Mo}_2\text{O}_2\text{S}_2(\text{L}^5)_2]$ | 2.868 | 1.714 1.715 | 2.159 2.161 | 2.342 2.350 2.352 2.324 | 2.501 2.504 | 1.748 1.751 | 1.349 1.345 |
| <i>trans</i> - $[\text{Mo}_2\text{O}_2\text{S}_2(\text{L}^5)_2]$ | 2.852 | 1.716 1.715 | 2.179 2.161 | 2.370 2.322 2.372 | 2.465 2.488 | 1.755 1.767 | 1.345 1.338 |

is dissolved in 40 mL of EtOH at 55–60 °C. Freshly prepared 25 mL of aqueous solution of $K_{2-x}(NMe_4)_x[I_2Mo_{10}O_{10}S_{10}(OH)_{10}(H_2O)_5] \cdot 2\text{H}_2\text{O}$ precursor (250 mg, 0.0833 mmol; 0.417 mmol $[\text{Mo}_2\text{O}_2\text{S}_2(\text{H}_2\text{O})_6]^{2+}$ is transferred to the hot thiosemicarbazone solution by dropwise addition. The mixture is stirred continuously and heated to 65 °C for one hour, which leads to the formation of yellow powders. For each synthesis, the yellow product is filtered, washed with water, ethanol, and diethyl ether, and then dried under vacuum. Through the diffusion method, using DMSO/EtOH:H₂O(1:1) it was possible to crystallize only one complex $[\text{Mo}_2\text{O}_2\text{S}_2(\text{HL}^3)_2]$.

$[\text{Mo}_2\text{O}_2\text{S}_2(\text{L}^1)_2]$. Yellow powder (yield = 90%). FT-IR/cm⁻¹, (Diamond ATR): 3368 (m); 3336 (m); 2933 (s); 2912 (s); 1579 (vw, sh.); 1447 (s); 1428 (s); 1353 (m); 1296 (vs); 1169 (s); 1072 (m); 1014 (s); 965 (vw, sh.); 951 (m); 901 (vs); 846 (s); 824 (s); 727 (m); 689 (m); 660 (s); 578 (s); 474 (s). ¹H RMN: δ ppm (300 MHz/DMSO-d₆): 9.52 (m, 1H); 9.18 (s, 1H); 7.72 (s, 2H); 7.16 (s, 1H); 3.02 (d, 3H); 2.37 (s, 6H). Elemental analysis for $[\text{Mo}_2\text{O}_2\text{S}_2(\text{C}_{11}\text{H}_{14}\text{N}_3\text{S}_2)]$ Calc. (found): C 36.26 (36.24); H 3.87 (3.65); N 11.53 (11.46); S 17.60 (17.46). EDX: found (expected): Mo/S = 0.51 (0.50). MALDI-TOF: m/z Calc. (found) 729.6 (729.9) for molecular ion $[\text{M} + \text{H}]^+$ and m/z 751.6 (751.9) for $[\text{M} + \text{Na}]^+$.

$[\text{Mo}_2\text{O}_2\text{S}_2(\text{L}^2)_2]$. Yellow powder (yield = 96%). FT-IR/cm⁻¹, (Diamond ATR): 3499 (m); 3438 (m); 3375 (w); 3325 (m); 1592 (vw, sh.); 1505 (w); 1380 (vs); 1350 (w); 1289 (s); 1163 (s); 1051 (s); 955 (vw, sh.); 848 (s); 813 (vs); 797 (vs); 731 (s); 693 (s); 685 (s); 561 (vs); 550 (vs); 538 (vs); 481 (s); 458 (s). ¹H RMN: δ ppm (300 MHz/DMSO-d₆): 9.21 (d, 1H); 9.16 (s, 2H); 7.73 (s, 1H); 7.16 (s, 1H); 2.36 (s, 6H). Elemental analysis for $[\text{Mo}_2\text{O}_2\text{S}_2(\text{C}_{10}\text{H}_{12}\text{N}_3\text{S}_2)]$ Calc. (found): C 34.29 (34.12); H 3.45 (3.30); N 12.00 (11.81); S 18.31 (18.37). EDX expected (found): Mo/S = 0.48 (0.50). MALDI-TOF: m/z Calc. (found) 701.6 (701.9) for $[\text{M} + \text{H}]^+$ and m/z 723.6 (723.9) for $[\text{M} + \text{Na}]^+$.

$[\text{Mo}_2\text{O}_2\text{S}_2(\text{HL}^3)_2]$. Yellow powder (yield = 63%). FT-IR/cm⁻¹, (Diamond ATR): 3339 (s); 3306 (w); 1595 (m, br.); 1554 (w, br.); 1527 (w, br.); 1478 (w); 1448 (w); 1387 (vs); 1360 (s); 1331 (s); 1259 (w, br.); 1216 (w); 1186 (s); 1166 (s); 1108 (s); 1067 (w); 957 (m); 931 (m); 882 (vs); 830 (vs); 807 (s); 784 (s); 755 (vs); 736 (m); 642 (s); 610 (s); 571 (m); 537 (s); 523 (s); 479 (s). ¹H RMN: δ ppm (300 MHz/DMSO-d₆): 9.62–9.34 (m, 3H); 7.77 (d, 1H); 7.10 (d, 1H); 6.91 (t, 1H); 3.88 (s, 3H); 3.00 (d, 3H). Elemental analysis for $[\text{Mo}_2\text{O}_2\text{S}_2(\text{C}_{10}\text{H}_{12}\text{N}_3\text{SO}_2)]$ ($\text{Mo}_{12}\text{O}_{12}\text{S}_{12}(\text{OH})_{12}(\text{H}_2\text{O})_6\right)_{0.035}(\text{CH}_3\text{OH})_{0.5}(\text{H}_2\text{O})_{0.5}$ Calc. (found): C

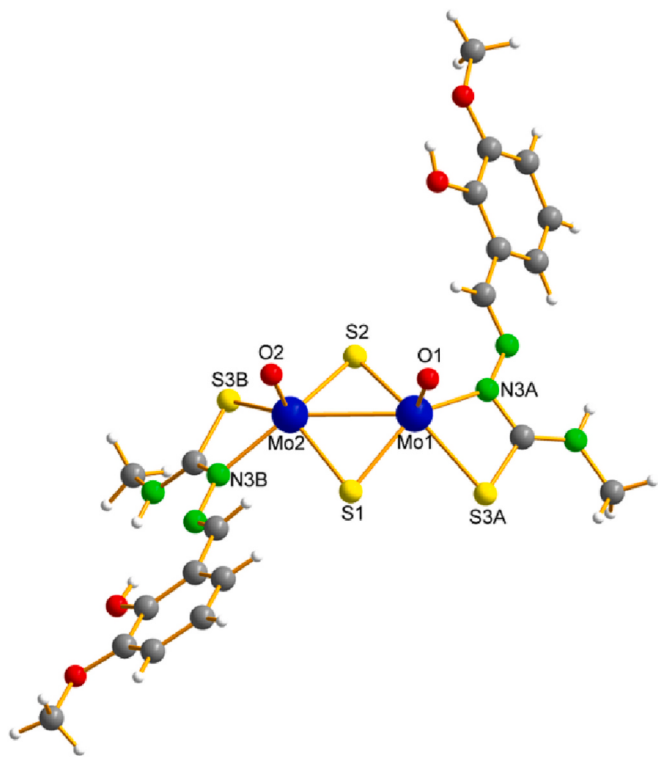


Fig. 3. X-Ray molecular structure of $[\text{Mo}_2\text{O}_2\text{S}_2(\text{HL}^3)_2]$ complex. Colour code: Mo (blue), C (grey), O (red), N (green), and S (yellow). (For interpretation of the references to colour in this figure legend, the reader is referred to the web version of this article.)

28.60 (28.73); H 3.26 (3.01); N 9.76 (9.96); S 16.46 (16.26). EDX found (expected): Mo/S = 0.53 (0.50). MALDI-TOF: m/z Calc. (found) 765.6 (765.8) for $[\text{M} + \text{H}]^+$ and m/z 787.6 (787.8) for $[\text{M} + \text{Na}]^+$.

$[\text{Mo}_2\text{O}_2\text{S}_2(\text{HL}^4)_2]$. Yellow powder (yield = 76%). FT-IR/cm⁻¹, (Diamond ATR): 3464 (vs); 3247 (vs); 1603 (vw, sh.); 1571 (s); 1493 (w); 1467 (vs); 1451 (vs); 1402 (s); 1333 (m); 1268 (vw); 1220 (vs); 1185 (s); 1164 (s); 1083 (s); 1040 (m); 1021 (s); 963 (m); 950 (m); 865 (vs); 838 (vs); 817 (m); 780 (s); 766 (s); 736 (m); 687 (s); 653 (vs); 596 (vs); 570 (vs); 532 (vs); 477 (s); 394 (s); 342 (s). ^1H RMN: δ ppm (300 MHz/DMSO-*d*₆): 9.81 (s, 1H); 9.56 (q, 1H); 9.49 (s, 1H); 7.71 (d, 1H); 7.00–6.89 (m, 2H); 3.79 (s, 3H); 3.01 (d, 3H). Elemental analysis for $[\text{Mo}_2\text{O}_2\text{S}_2(\text{C}_{10}\text{H}_{12}\text{N}_3\text{SO}_2)_2]$ ($\text{Mo}_{12}\text{O}_{12}\text{S}_{12}(\text{OH})_{12}(\text{H}_2\text{O})_6$)_{0.019}(CH₃OH)_{0.8}(H₂O)_{2.5} Calc. (found): C 28.30 (28.58); H 3.71 (3.77); N 9.92 (9.62); S 15.22 (12.51). EDX found (expected): Mo/S = 0.52 (0.50). MALDI-TOF: m/z Calc. (found) 765.6 (765.8) for $[\text{M} + \text{H}]^+$ and m/z 787.6 (787.8) for $[\text{M} + \text{Na}]^+$.

$[\text{Mo}_2\text{O}_2\text{S}_2(\text{L}^5)_2]$. Yellow powder (yield = 92%). FT-IR/cm⁻¹, (Diamond ATR): 3296 (s); 3027 (vs); 1589 (vw, sh.); 1508 (s); 1488 (w); 1363 (vs); 1320 (s); 1282 (m); 1269 (m); 1174 (vs); 1079 (s); 1029 (vs); 960 (w); 945 (s); 839 (s); 808 (s); 751 (m); 729 (vs); 714 (vs); 698 (m); 669 (m); 637 (s); 617 (s); 598 (s); 547 (s); 533 (s). ^1H RMN: δ ppm (300 MHz/DMSO-*d*₆): 9.47 (m, 1H); 9.13 (s, 1H); 7.97 (d, 2H); 7.38 (t, 4H); 7.14 (d, 4H); 7.10 (d, 2H); 7.02 (d, 4H); 2.99 (d, 3H). Elemental analysis for $[\text{Mo}_2\text{O}_2\text{S}_2(\text{C}_{21}\text{H}_{19}\text{N}_4\text{S})_2]$ Calc. (found): C 50.10 (49.97); H 3.80 (3.88); N 11.13 (11.07); S 12.74 (12.81). EDX found (expected): Mo/S = 0.46 (0.50). MALDI-TOF: m/z Calc. (found) 1007.9 (1007.9) for $[\text{M} + \text{H}]^+$ and m/z 1029.9 (1029.9) for $[\text{M} + \text{Na}]^+$.

Fig. S1 depicts the FT-IR spectra of complexes, while MALDI-TOF spectra given in Fig. 2 and in Figs. S7–S10 in supporting information. ^1H NMR data and spectra can be found in Table S1 and in Fig. 4 and Figs. S17–S20.

3. Results

3.1. Synthesis

The cyclic compound $\text{K}_{2-x}(\text{NMe}_4)_x[\text{I}_2\text{Mo}_{10}\text{O}_{10}\text{S}_{10}(\text{OH})_{10}(\text{H}_2\text{O})_5]$ (denoted Mo_{10}) is used as precursor to obtain the $[\text{Mo}_2^{(\text{V})}\text{O}_2\text{S}_2]^{2+}$ cluster. This family of molybdenum cycles are highly labile [46]. Therefore, the Mo_{10} solution must be prepared quickly and immediately mixed with ligands because Mo_{10} precursor can quickly reorganize to give the neutral insoluble compound $[\text{Mo}_{12}\text{O}_{12}\text{S}_{12}(\text{OH})_{12}(\text{H}_2\text{O})_6]$ [47]. This Mo_{10} cycle possesses 10 hydroxo bridges, which can deprotonate thiosemicarbazone ligands in the water/ethanol reaction medium. Quantitatively, 10 OH^- bridges can react with 10 molecules of thiosemicarbazone ligands. During the hydrolysis of the cycle, 5 fragments of $[\text{Mo}_2\text{O}_2\text{S}_2]^{2+}$ are obtained which react with the mono-deprotonated ligands. As can be seen in Scheme 1, thiosemicarbazone ligands can exist in two forms. It is well known that uncoordinated ligands adopt the thione form (form A in Scheme 1). However, deprotonation generally takes place on the azomethine nitrogen atom, and the coordination of the ligand then takes place in the deprotonated thiolate form B. In this study, we obtained 5 compounds in powder form, which were characterized by FT-IR (see Fig. S1, SI), Elemental Analysis and EDX. These analyses agree with the formation of complexes between the $[\text{Mo}_2\text{O}_2\text{S}_2]^{2+}$ cluster and the monodeprotonated thiosemicarbazone ligands and in particular the formation of neutral complexes of the $[\text{Mo}_2\text{O}_2\text{S}_2(\text{H}_n\text{L})_2]$ type. Mass spectrometry by the MALDI-TOF method is thus carried out to confirm the stoichiometry in these complexes (see Figs. S7–S10, SI).

3.2. FT-IR spectra

The FT-IR spectra of the thiosemicarbazone ligands exhibit a strong band in the 3392–3294 cm⁻¹ region, which is attributed to the -NH-group or two bands in the case of the terminal -NH₂ group. The absorption frequencies of the imine group $\nu(\text{C}=\text{N})$ around 1600–1550 cm⁻¹ appear as very strong bands and the bands corresponding to $\nu(\text{C}=\text{S})$ are of medium intensity in a wide range 800–1000 cm⁻¹. Upon coordination with the cluster $[\text{Mo}_2\text{O}_2\text{S}_2]^{2+}$, the vibrations bands associated to the -NH- group and the $\nu(\text{C}=\text{S})$ of the ligand disappear, while significant shifts of the vibrations bands of the ligands are observed (see Fig. S1, SI). Furthermore, the presence of the $[\text{Mo}_2\text{O}_2\text{S}_2]^{2+}$ fragment is evidenced by the strong vibration band around 950–960 cm⁻¹. Besides, for ligands H_2L^3 and H_2L^4 , the FT-IR spectra present a broad band at approximately 3380 cm⁻¹ attributed to the phenolic group, $\nu(\text{OH})$, which does not disappear from the spectra of the complexes, in agreement with X-Ray structure of $[\text{Mo}_2\text{O}_2\text{S}_2(\text{HL}^3)_2]$ and $[\text{Mo}_2\text{O}_2\text{S}_2(\text{HL}^4)_2]$ evidencing the phenol group of the ligands remain protonated and uncoordinated in the complexes.

3.3. MALDI-TOF

MALDI-TOF mass spectrometry has proven to be very effective in characterizing such neutral complexes. The results obtained for our 5 complexes are gathered in Table 2. Fig. 2 shows an example of a spectrum obtained for the compound $[\text{Mo}_2\text{O}_2\text{S}_2(\text{HL}^3)_2]$, while the spectra obtained for complexes $[\text{Mo}_2\text{O}_2\text{S}_2(\text{L}^1)_2]$, $[\text{Mo}_2\text{O}_2\text{S}_2(\text{L}^2)_2]$, $[\text{Mo}_2\text{O}_2\text{S}_2(\text{HL}^4)_2]$, and $[\text{Mo}_2\text{O}_2\text{S}_2(\text{L}^5)_2]$ are given in Figs. S7 to S10, respectively (Supporting Information). The complexes obtained are neutral. In all cases, only a few degradation products are observed, and the main peaks correspond to monocationic adducts formed between the expected neutral complexes and an H^+ proton or a Na^+ cation. The simulated isotopic distribution perfectly matches the 1:2 stoichiometry of $[\text{Mo}_2\text{O}_2\text{S}_2(\text{L})_2]$ complexes, in agreement with previous studies by Fuior et al. [33].

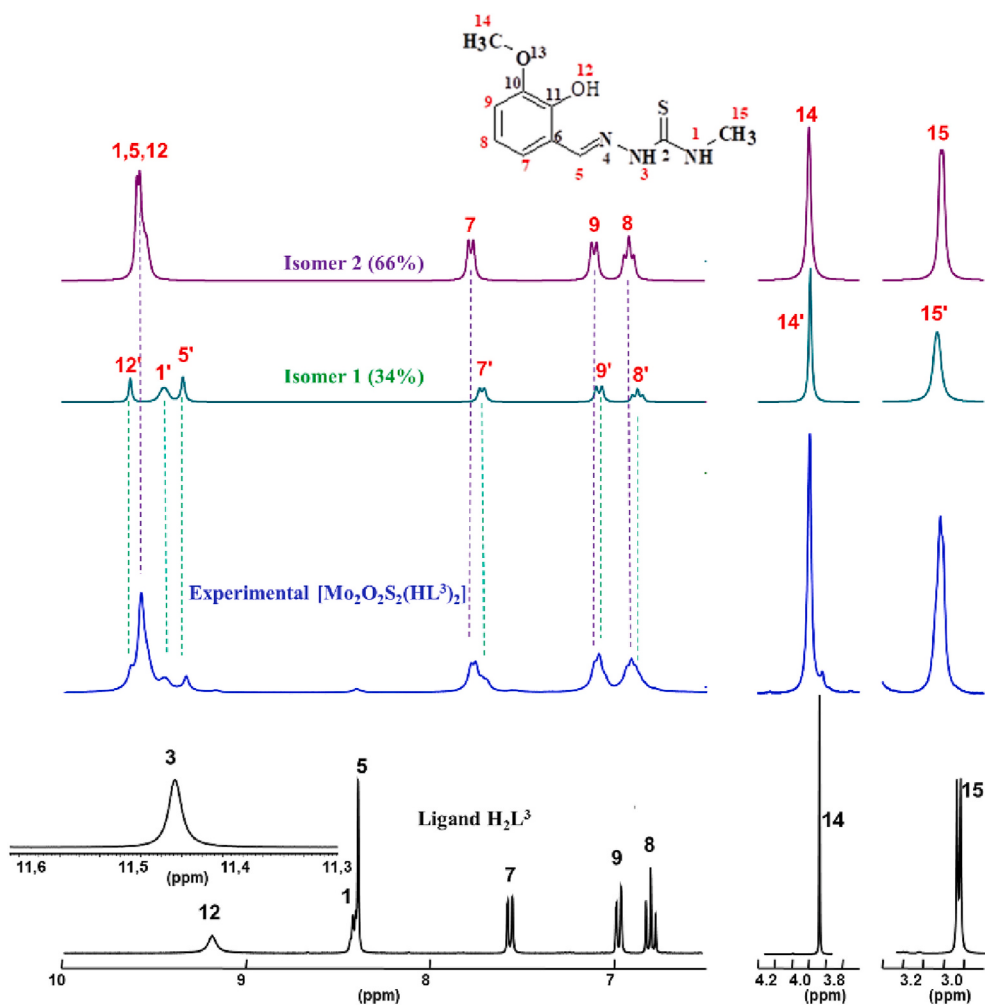


Fig. 4. ^1H NMR (DMSO-d_6 , 300 MHz) spectra of ligand H_2L^3 (black), complex $[\text{Mo}_2\text{O}_2\text{S}_2(\text{HL}^3)_2]$ (blue) at 10^{-2} M, and the simulated subspectra contained in the experimental spectrum of $[\text{Mo}_2\text{O}_2\text{S}_2(\text{HL}^3)_2]$. (For interpretation of the references to colour in this figure legend, the reader is referred to the web version of this article.)

3.4. X-ray crystal structure

The $[\text{Mo}_2\text{O}_2\text{S}_2(\text{HL}^3)_2]$ complex solvated with two DMSO molecules crystallizes in a triclinic $\overline{\text{P}1}$ space group. The detailed crystallographic data are given in Table 1 and selected distances are listed in Table 3. The molecular structure of the complex is depicted in the Fig. 3. The two monodeprotonated bidentate thioureas are coordinated in *trans* configuration to $[\text{Mo}_2^{(\text{V})}\text{O}_2\text{S}_2]^{2+}$ cluster, through S-thiolate and azomethinic N atoms. This type of coordination leads to a 4-atom ring with Mo(V) metal ions, where the Mo—S and Mo—N distances were found to be 2.441 and 2.136 Å, respectively. The phenolic and imino groups are not involved in coordination conversely to what usually happens in 3d complexes. Both Mo(V) atoms in $[\text{Mo}_2^{(\text{V})}\text{O}_2\text{S}_2]^{2+}$ cluster are pentacoordinated with a distorted square pyramidal geometry. The Mo—Mo (2.831 Å), Mo—S (2.302–2.341 Å) and Mo=O (1.675–1.678 Å) bond distances are consistent with the usual ranges observed in the $[\text{Mo}_2^{(\text{V})}\text{O}_2\text{S}_2]^{2+}$ cluster [46,48,49]. The deprotonation of the ligand is confirmed by C—S and C=N bond distances. Thus, the increase in the distance of the C—S bond (1.745 Å) in the complex compared to the C=S in the free ligand (1.695 Å) is accompanied by a shortening of the C—N bond (1.338 Å) between the azomethinic C and the hydrazinic N atoms in the complex compared to C=N double bond in the uncoordinated ligand (1.363 Å) [50]. The crystal packing of the complex is stabilized by intermolecular bonding between DMSO molecules and molecular units (Fig. S11, ESI). The oxygen atom of one DMSO

molecule is connecting two molecular units by hydrogen bonds with phenol and amino groups: $\text{H12A}_{(\text{OH})}\dots\text{O1D}_{(\text{DMSO})}\dots\text{H1A}_{(\text{NHMe})}$ (2.028 and 1.971 Å, respectively). These dimeric assemblies end with hydrogen bonding between oxygen atom of second DMSO molecule and phenol and amino groups of one molecular unit, $\text{H12B}_{(\text{OH})}\dots\text{O1C}_{(\text{DMSO})}\dots\text{H1B}_{(\text{NHMe})}$ (2.663 and 1.977 Å respectively).

3.5. NMR studies

^1H NMR spectra of free ligands and complexes were recorded in DMSO. The example of $[\text{Mo}_2\text{O}_2\text{S}_2(\text{HL}^3)_2]$ complex at 10^{-2} M is given in Fig. 4, while the spectra of all other ligands and complexes at 10^{-2} M are given in the Supporting Information (Fig. S17–S20). The chemical shifts of the ligands and complexes are reported in Table S1 in the Supporting Information. As a general feature, the ^1H NMR spectra of the complexes clearly confirm the deprotonation of the N azomethine NH group of the ligands and the coordination of the ligands to the Mo(V) cluster $[\text{Mo}_2^{(\text{V})}\text{O}_2\text{S}_2]^{2+}$. It is worth mentioning that the latter is diamagnetic due to the Mo—Mo bond that realizes the pairing of the two lone electrons in each metal centre. The analysis of the ^1H NMR spectra also confirms that the OH functions in the two ligands H_2L^3 and H_2L^4 remain protonated and are not coordinated to Mo, in agreement with Fiuor et al. [33]. In this previous study, it was shown that depending on the different substituents in position R^3 and R^4 , up to 8 isomers can be obtained in solution. We hypothesized that using $\text{R}^3 = \text{H}$ and $\text{R}^4 = \text{H}$ or alkyl should

Table 4

Total Bonding Energies in $\text{kcal}\cdot\text{mol}^{-1}$, HOMO, LUMO and HOMO-LUMO gap energies in eV for ligands (as protonated ligand) and complexes in *cis* and *trans* configurations.

| Molecule | Total Bonding Energy ($\text{kcal}\cdot\text{mol}^{-1}$) | $\Delta E_{\text{cis-trans}} = E_{\text{trans}} - E_{\text{cis}}$ ($\text{kcal}\cdot\text{mol}^{-1}$) | HOMO (eV) | LUMO (eV) | HOMO-LUMO gap (eV) |
|---|--|---|-----------|-----------|--------------------|
| Model <i>cis</i> | -4589.87 | | -5.703 | -3.141 | 2.562 |
| Model <i>trans</i> | -4590.52 | -0.65 | -5.773 | -3.224 | 2.549 |
| HL ¹ | -4159.18 | | -5.40 | -2.67 | 2.73 |
| <i>cis</i> -[Mo ₂ O ₂ S ₂ (L ¹) ₂] | -9244.78 | | -5.47 | -3.07 | 2.40 |
| <i>trans</i> -[Mo ₂ O ₂ S ₂ (L ¹) ₂] | -9243.95 | +0.83 | -5.50 | -3.15 | 2.35 |
| HL ² | -3789.30 | | -5.45 | -2.71 | 2.74 |
| <i>cis</i> -[Mo ₂ O ₂ S ₂ (L ²) ₂] | -8502.55 | | -5.55 | -3.11 | 2.44 |
| <i>trans</i> -[Mo ₂ O ₂ S ₂ (L ²) ₂] | -8502.00 | +0.55 | -5.59 | -3.27 | 2.32 |
| HL ³ | -4076.03 | | -5.28 | -2.58 | 2.70 |
| Conf. 1 | | | -5.47 | -3.20 | 2.27 |
| <i>cis</i> -[Mo ₂ O ₂ S ₂ (L ³) ₂] | -9064.45 | -8.02 | | | |
| Conf. 1 | -9072.47 | | -5.35 | -3.17 | 2.16 |
| <i>trans</i> -[Mo ₂ O ₂ S ₂ (L ³) ₂] | -9071.20 | | -5.53 | -3.15 | 2.38 |
| Conf. 2 | | -8.41 | | | |
| <i>cis</i> -[Mo ₂ O ₂ S ₂ (L ³) ₂] | -9079.61 | | -5.32 | -3.18 | 2.14 |
| Conf. 2 | | | -5.52 | -3.17 | 2.35 |
| <i>cis</i> -[Mo ₂ O ₂ S ₂ (L ³) ₂] | -9079.79 | -3.98 | -5.29 | -3.20 | 2.09 |
| Conf. 3 | | | -5.11 | -2.70 | 2.41 |
| <i>trans</i> -[Mo ₂ O ₂ S ₂ (L ³) ₂] | -9083.77 | | -5.12 | -3.13 | 1.99 |
| HL ⁴ | -4075.29 | | -5.14 | -3.17 | 1.97 |
| (Conf.3) | | | -4.79 | -2.64 | 2.15 |
| <i>cis</i> -[Mo ₂ O ₂ S ₂ (L ⁴) ₂] | -9087.44 | | -4.81 | -3.05 | 1.76 |
| (Conf.1) | | +11.49 | | | |
| <i>trans</i> -[Mo ₂ O ₂ S ₂ (L ⁴) ₂] | -9075.95 | | -4.83 | -3.17 | 1.66 |
| HL ⁵ | -6793.26 | | -4.86 | -1.52 | 3.33 |
| <i>cis</i> -[Mo ₂ O ₂ S ₂ (L ⁵) ₂] | -14,519.90 | +11.74 | -5.59 | -3.07 | 2.52 |
| <i>trans</i> -[Mo ₂ O ₂ S ₂ (L ⁵) ₂] | -14,508.16 | | | | |
| Trolox | -5021.40 | | | | |
| Rutin | -10,494.76 | | | | |

limit the number of isomers to at least 2. Moreover, in the present study, the series of 5 ligands aimed to put larger substituents in R¹ or R² to promote the formation of a single isomer due to a steric hindrance between the ligands.

The analysis of the ¹H NMR spectra of the 5 complexes of this study confirms the first hypothesis but it does not allow to form only one species in solution. All spectra can be mainly decomposed into two subspectra displaying the same multiplicities in DMSO. These two sets of NMR signals are assigned to two distinct complexes which are attributed to the *cis* and *trans* isomers of the complexes.

The proportions of the various isomers are indicated on the ¹H NMR spectra and at this stage it is difficult to discriminate between the *cis* and *trans* isomers in solution. For example, in the case of the [Mo₂O₂S₂(HL³)₂] complex, the species distribution for H₂L³ was 66:34 for isomer2:isomer1. It was not possible to determine which spectrum corresponds to the *cis* isomer and which spectrum corresponds to the *trans* isomer. These proportions of isomers are found equal to 64:36 for [Mo₂O₂S₂(L¹)₂] (Fig. S17, SI), 63:37 for [Mo₂O₂S₂(L²)₂] (Fig. S18, SI), 83:17 for [Mo₂O₂S₂(HL⁴)₂] (Fig. S19, SI), and 41:59 for [Mo₂O₂S₂(L⁵)₂] (Fig. S20, SI). Interestingly, when concentration is relatively high (10⁻² M), the ¹H NMR spectra display almost only the signals of the two isomers but when the concentration decreases (5.10⁻³ and lower), a small amount of uncoordinated ligand appears (5–8% for all complexes at 5 mM concentration as shown in Figs. S22–S26, SI), indicating a partial decoordination when the complexes are diluted. This phenomenon increases when concentration diminishes, according to the Ostwald Law (see Fig. S21, SI). These results suggest that at high concentration, the biological activity can be due to the initial complexes but at low concentration it must result from partially decomposed complexes. Furthermore, at a given concentration (5 mM), the proportions of species do not vary within at least 72 h as shown in Fig. S22–S26 (SI), meaning that no dynamic equilibrium between isomers occurs. DFT

calculations were then undertaken on all possible *cis/trans* species, and their conformers aimed at understanding these results.

3.6. DFT studies

In the absence of additional structural data and aiming to shed light into the preferential formation of *cis* or *trans* isomers, the molecular geometries of all ligands, complexes and a model system were fully optimized by means of a DFT method (see above). We considered a model complex, which consist of the simplest thiosemicarbazone-Mo₂O₂S₂ complex, to assess the energy difference between the *cis* and *trans* conformations in the absence of ligands effects (see Fig. S27, SI). This preference turned to be quite low (0.65 $\text{kcal}\cdot\text{mol}^{-1}$) favouring the *trans* isomer (Table 4).

The series of complexes can be classified in three groups depending on the ligand structure. In the first group we can align ligand HL¹ and HL² as well as their respective metal complexes. Both HL¹ and HL² have similar structures, differing one of the other on the CH₃ on the N¹ position. None of these structures can form intramolecular hydrogen bonds. Second group is formed by H₂L³ and H₂L⁴ ligands and their metal complexes. Both ligands can form 0, 1 or 2 intramolecular OH-N hydrogen bonds. For this reason, we considered three different conformers for each [Mo₂O₂S₂(HL³)₂] *cis* and *trans* complexes: conformer 1 (Conf. 1) present zero hydrogen bonds, conformer 2 (Conf. 2) one, and conformer 3 (Conf. 3) two (see Fig. S28, SI). The last group includes HL⁵ and its metal complexes. In this case, there is no possibility of intramolecular hydrogen bonds, but some π stacking interactions between aromatic rings are possible at the same time.

The *cis* complexes formed with ligands HL¹ and HL² are flexible enough to give or not give π-π stacking between aromatic groups in the substituents R¹ (see Fig. 5). Consequently, for the [Mo₂O₂S₂(L¹)₂] complex, we also considered two different conformers, one with the

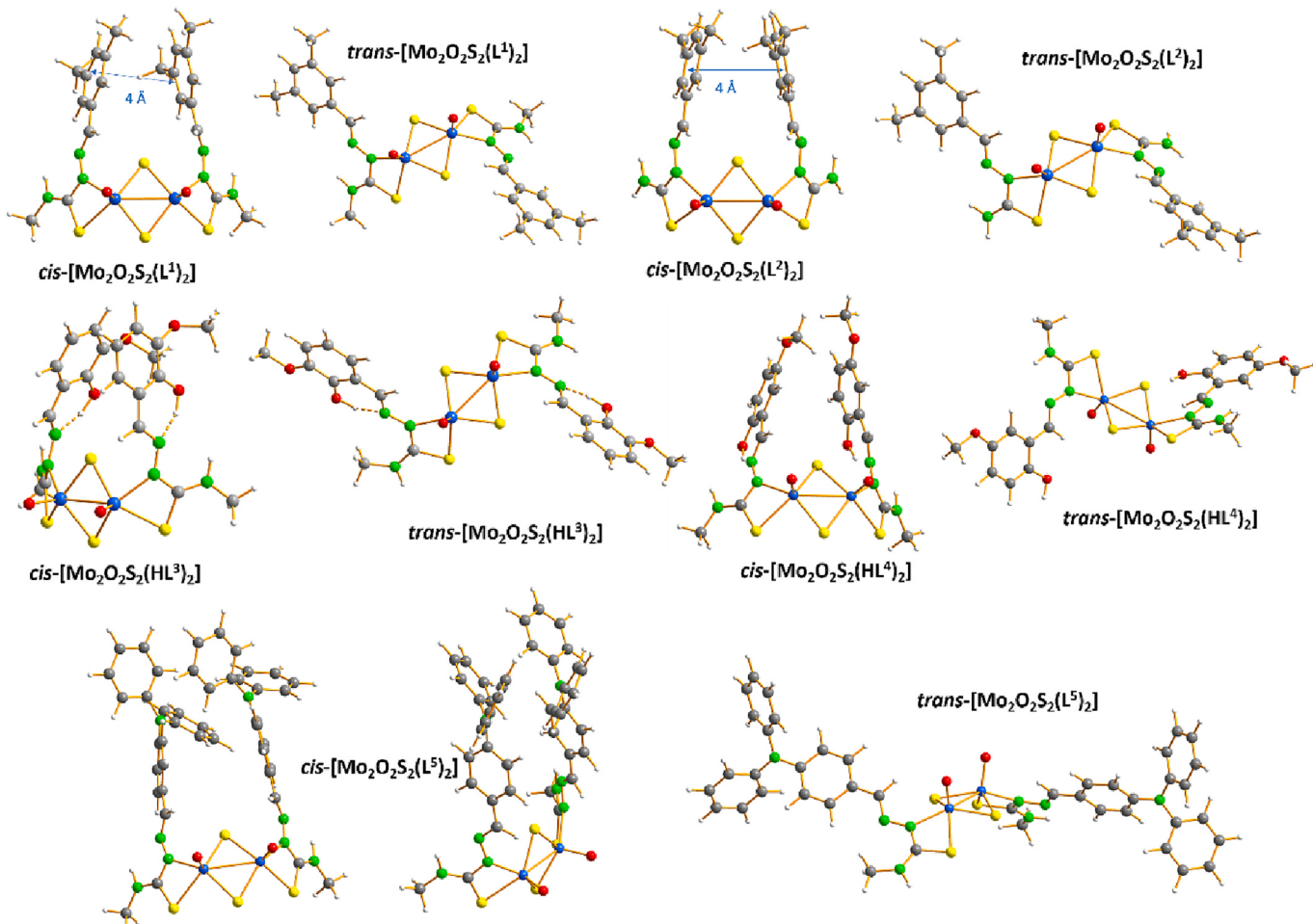


Fig. 5. DFT optimized molecular structures of complexes in *cis* and *trans* configurations. Colour code: Mo (blue), C (grey), O (red), N (green), and S (yellow). (For interpretation of the references to colour in this figure legend, the reader is referred to the web version of this article.)

rings in parallel position and the other with a CH₃ group pointing towards the centre of the opposite ring. Results of this calculations show no major differences (0.2 kcal·mol⁻¹). The same difference in energy is found in HL² *cis* complex. Regarding the *cis* / *trans* preference of [Mo₂O₂S₂(L¹)₂] and [Mo₂O₂S₂(L²)₂], the data in Table 4 indicates that both species are in equilibrium, with a small preference for the *cis* isomer in both cases.

The X-Ray characterized complex [Mo₂O₂S₂(HL³)₂] shows the *trans* disposition, and regarding intramolecular presents conformation Conf.2 as described above, so one OH-N hydrogen bond (see Fig. 3 and Fig. S28, SI). We considered the three different conformers. The optimized geometries for the complexes in their two most stable isomeric forms are depicted in Fig. 5, while selected distances are given in Table 3 in comparison with experimental values. What it can be deduced from Table 3, is that the bond distances obtained by DFT fully agree with the experimental data obtained for compound [Mo₂O₂S₂(HL³)₂], and also with the previous complexes reported by Fuior et al. [33]. In particular, the Mo–Mo distances are fully compatible with a Mo–Mo bond expected for the [Mo^(V)O₂S₂]²⁺ cluster. This good agreement validates the molecular structures obtained by DFT geometrical optimization. π–π interactions are also found in the *cis*-[Mo₂O₂S₂(HL³)₂] and *cis*-[Mo₂O₂S₂(HL⁴)₂] complexes in addition to the strong intramolecular H-bonds ($d_{OH-N} = 1.6\text{--}1.7 \text{ \AA}$) between the non-coordinated phenol groups and iminic N atoms of the ligands. As expected, in all cases the most stable conformers of the *cis* and *trans* complexes are the ones that have two intramolecular hydrogen bonds labelled Conf.3. The preference for the *trans* is small (4 kcal·mol⁻¹) and agreement with the X-Ray structure.

The difference between Conf.2 and Conf.3 is also small and could be easily overcome by packing effects. Considering the small energies in play, a solvent like DMSO might interrupt the stabilizing intermolecular interactions and make the *cis* and *trans* complexes equally stable. For [Mo₂O₂S₂(HL⁴)₂] we report Conf. 3 for the *cis* and Conf. 1 for the *trans*, to show how important are the presence of intermolecular interactions in the stability of those complexes.

For complex *cis*-[Mo₂O₂S₂(L⁵)₂], which includes the bulkiest ligand, the three phenyl groups of the one ligand stand parallel to those of the second ligand with C–C distances in the 3.5–3.7 Å range, a distance compatible with π–π stacking interactions between both ligands in this conformation. This stabilizing intramolecular interaction could not exist in the *trans* isomer. Therefore, this would explain why *cis*-[Mo₂O₂S₂(L⁵)₂] is thermodynamically more stable than *trans*-[Mo₂O₂S₂(L⁵)₂].

For all cases bonding energies show that *cis* / *trans* isomers seem to be in an equilibrium with their corresponding conformers. Intuitively, introducing bulky substituents at the R¹ position in the ligand should increase the steric constraints between the ligands once complexed into the *cis* isomer and thus favour the formation of the *trans* isomer. In fact, as shown in Fig. 5, the two ligands are not that close and stabilizing intramolecular interactions such as π–π stacking interaction between the two ligands are only found in the *cis* isomers, counteracting possible steric repulsions.

Prediction of ¹H NMR spectra were performed for HL¹ and HL³ ligand and its *cis* and *trans* isomers. Chemical shifts for the different hydrogen's signals are collected in Table 5 in comparison with isomers 1

Table 5

Experimental and calculated chemicals shifts (in ppm) for HL^1 and H_2L^3 ligands and their metal complexes. Note that for some complexes both ligands are not identical. In this case, two/three sets of chemical shifts are obtained.

| | | | H(1) | H(3) | H(5) | H(7) | H(8) | H(9) | H(10) | H(11) | H(12) | H(14) | H(15) |
|----------------|-----|---|-------------|-------|-------------|-----------------|------|-------------|-------------|-------|--------------|-------|-------|
| NMR | DFT | HL^1 | 8.6 | 9.5 | 8.2 | 7.7/8.4 | — | 7.8 | 2.7/ 2.8 | 3.7 | — | — | — |
| | | Cis- $[\text{Mo}_2\text{O}_2\text{S}_2(\text{L}^1)_2]$ | 8.5/ 8.7 | — | 9.6/ 9.8 | 7.8/ 8.2/8.4 | — | 7.7/ 8.0 | 2.7/ 3.0 | 3.5 | — | — | — |
| | | trans- $[\text{Mo}_2\text{O}_2\text{S}_2(\text{L}^1)_2]$ | 8.8/ 8.9 | — | 9.4/ 9.5 | 8.1/8.7 | — | 8.0 | 2.9 | 3.5 | — | — | — |
| | | HL^1 | 8.45 | 11.43 | 7.98 | 7.39 | — | 7.03 | 2.28 | 3.02 | — | — | — |
| | | Isomer 1 | 9.41 | 9.35 | 7.73 | — | — | 7.12 | 2.34 | 3.04 | — | — | — |
| | | Isomer 2 | 9.52 | 9.19 | 7.71 | — | — | 7.17 | 2.38 | 3.02 | — | — | — |
| | | HL^3 | 6.5 | 9.3 | 8.5 | 7.4 | 7.4 | 7.4 | — | — | 14.1 | 4.2 | 3.2 |
| | | Conf 1 | — | — | — | — | — | — | — | — | — | — | — |
| | | cis- $[\text{Mo}_2\text{O}_2\text{S}_2(\text{L}^3)_2]$ | 8.2 | — | 9.8 | 8.3 | 7.4 | 7.6 | — | — | 6.6 | 4.4 | 3.3 |
| | | Conf 1 | — | — | — | — | — | — | — | — | — | — | — |
| NMR | DFT | trans- $[\text{Mo}_2\text{O}_2\text{S}_2(\text{L}^3)_2]$ | 7.3 | — | 9.8 | 8.0 | 7.5 | 7.5 | — | — | 6.9 | 4.2 | 3.5 |
| | | Conf 2 | — | — | — | — | — | — | — | — | — | — | — |
| | | cis- $[\text{Mo}_2\text{O}_2\text{S}_2(\text{L}^3)_2]$ | 7.6 | — | 9.6 | 7.5 | 7.2 | 7.7 | — | — | 13.0/ 6.3 | 4.3 | 3.1 |
| | | Conf 2 | — | — | — | — | — | — | — | — | — | — | — |
| | | trans- $[\text{Mo}_2\text{O}_2\text{S}_2(\text{L}^3)_2]$ | 6.8 | — | 9.5 | 7.8 | 7.5 | 7.5 | — | — | 13.3/ 7.0 | 4.2 | 3.6 |
| | | Conf 3 | — | — | — | — | — | — | — | — | — | — | — |
| | | cis- $[\text{Mo}_2\text{O}_2\text{S}_2(\text{L}^3)_2]$ | 7.6 | — | 9.4 | 7.6 | 7.2 | 7.6 | — | — | 12.8 | 4.2 | 3.2 |
| | | Conf 3 | — | — | — | — | — | — | — | — | — | — | — |
| | | HL^3 | 6.8 | — | 9.3 | 7.6 | 7.5 | 7.5 | — | — | 13.4 | 4.2 | 3.5 |
| | | Isomer 1 | 8.40 | 11.44 | 8.38 | 7.55 | 6.78 | 6.95 | — | — | 9.19 | 3.80 | 3.00 |
| | | Isomer 2 | 9.44 | — | 9.33 | 7.71 | 6.88 | 7.07 | — | — | 9.62 | 3.89 | 3.01 |
| | | Isomer 2 | 9.58 | — | 9.58 | 7.77 | 6.91 | 7.11 | — | — | 9.58 | 3.89 | 3.01 |

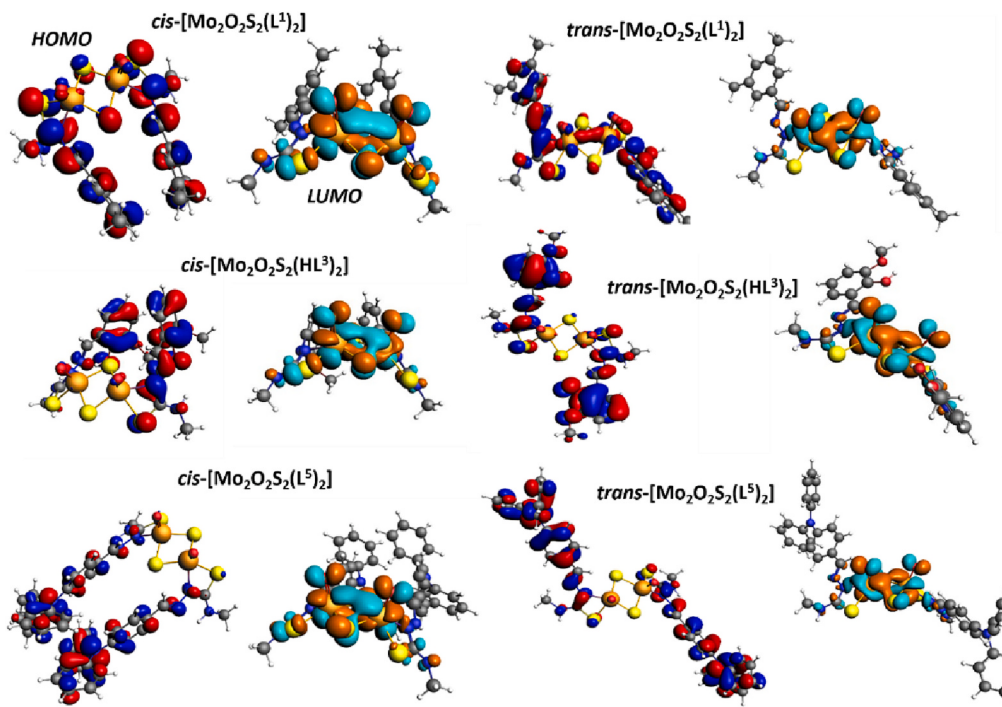


Fig. 6. Representation of the HOMO (left) and LUMO (right) frontiers orbitals for cis and trans isomers of complexes $[\text{Mo}_2\text{O}_2\text{S}_2(\text{L}^1)_2]$, $[\text{Mo}_2\text{O}_2\text{S}_2(\text{HL}^3)_2]$ and $[\text{Mo}_2\text{O}_2\text{S}_2(\text{L}^5)_2]$.

and 2 experimentally observed (see Fig. 4, Fig. S17 and Table S2, SI). Unfortunately, no major differences between the *cis* and *trans* isomers could be observed and DFT calculation cannot help to assign isomers on

the NMR spectra. On the other hand, important differences were found between the signals of different conformers. The existence of OH-N hydrogen bonds implies a huge displacement of the OH signal (H12),

Table 6

Results of antifungal activity against *Cryptococcus neoformans*. NA: No Activity; MIC: minimum inhibitory concentration; MFC: minimum fungicidal concentration; MFC/MIC: < 2 is fungicidal, >2 is fungistatic and ≥ 32 is resistant; FA: fungicidal activity.

| Product | <i>Cryptococcus neoformans</i> CECT 1043 | | | |
|---|--|--------------------|-------------|------------|
| | MIC, mg/ mL(μM) | MFC, mg/ mL(μM) | MFC/ MIC | FA |
| HL ¹ | NA | NA | — | — |
| [Mo ₂ O ₂ S ₂ (L ¹) ₂] | 0.008 (10.9) | 0.008 (10.9) | 1 | fungicidal |
| HL ² | NA | NA | — | — |
| [Mo ₂ O ₂ S ₂ (L ²) ₂] | 0.004 (5.7) | 0.004 (5.7) | 1 | fungicidal |
| H ₂ L ³ | NA | NA | — | — |
| [Mo ₂ O ₂ S ₂ (HL ³) ₂] | 0.016 (18.3) | 0.016 (18.3) | 1 | Fungicidal |
| H ₂ L ⁴ | NA | NA | — | — |
| [Mo ₂ O ₂ S ₂ (HL ⁴) ₂] | 0.016 (18.0) | 0.016 (18.0) | 1 | fungicidal |
| HL ⁵ | NA | NA | — | — |
| [Mo ₂ O ₂ S ₂ (L ⁵) ₂] | NA | NA | — | — |
| [Mo ₂ O ₂ S ₂ (LHis) ₂] [11] | 0.500 (779.6) | 0.500 (779.6) | 1 | fungicidal |
| K ₂ [Mo ₂ O ₂ S ₂ (LCys) ₂] [11] | NA | NA | — | — |
| K ₂ [Mo ₂ O ₂ S ₂ (HNTA) ₂] [11] | 0.250 (287.1) | 0.250 (287.1) | 1 | fungicidal |
| K ₂ [Mo ₂ O ₂ S ₂ (EDTA)] [11] | 0.016 (23.1) | 0.016 (23.1) | 1 | fungicidal |
| [Mo ₂ O ₂ S ₂ (L ^a) ₂] [34] | 0.002 (2.9) | — | — | — |
| [Mo ₂ O ₂ S ₂ (L ^b) ₂] [34] | 0.002 (2.8) | — | — | — |
| [Mo ₂ O ₂ S ₂ (HL ^c) ₂] [34] | 0.004 (5.7) | — | — | — |
| [Mo ₂ O ₂ S ₂ (H ₂ L ^d) ₂] [34] | 0.0005 (0.6) | — | — | — |
| [Mo ₂ O ₂ S ₂ (H ₂ L ^e) ₂] [34] | 0.004 (5.5) | — | — | — |
| [Mo ₂ O ₂ S ₂ (L ^m) ₂] [34] | 0.002 (2.9) | — | — | — |
| [Mo ₂ O ₂ S ₂ (L ⁿ) ₂] [34] | 0.031 (46.4) | — | — | — |
| Nystatin | 0.032 (34.5) | 0.032 (34.5) | 1 | fungicidal |

from 6 to 7 ppm for the cases without, to 12–14 ppm for hydrogen bonded protons. Therefore, in addition to the *cis/trans* isomerism the computed NMR data suggest that several conformers could be present in solution. The presence or absence of hydrogen bonds in positions N¹ and N³ largely affects the N—H signals. This could explain why there is a 2 ppm mismatch between DFT results and experimental chemical shifts for those exchangeable protons. DMSO solvent molecules interact both with the ligands and the metal complexes, as it is depicted in the crystal structure of trans-[Mo₂O₂S₂(L³)₂] complex indeed (see Fig. S11). The aprotic solvent DMSO is able to accept protons and can form different

hydrogen bonds with the N³ proton of the free ligands, and also with N¹ proton in both the ligand and the complexes. Overall, for the C—H protons, the computed chemical shifts reproduce rather well the experimental values.

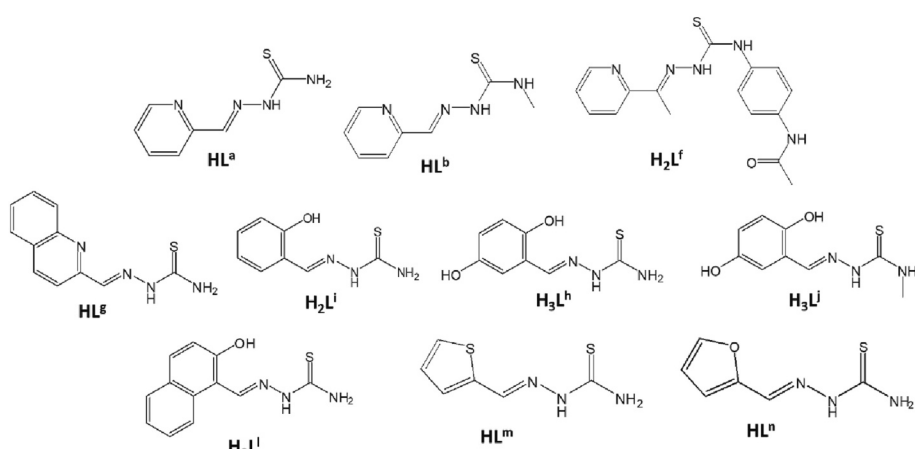
The HOMO and LUMO orbitals of ligands and complexes are depicted in Fig. 6 and Table S3 (Supporting Information). For complexes formed with ligands HL¹ and HL², the HOMO and LUMO orbitals are delocalized on the entire molecules, but the contribution of the ligands appears stronger for HOMO, while it is the reverse for the LUMO, which shows a stronger contribution on the cluster [Mo₂(V)O₂S₂]²⁺. In the case of the ligands H₂L³, H₂L⁴ and HL⁵, the difference between the ligand and the cluster is emphasized since the contribution of the cluster to the HOMO orbital becomes negligible while its contribution to the LUMO orbital becomes major. It means that the reduction of such complexes and thus the addition of electrons within the LUMO will mainly occur on the cluster while the oxidation, a loss of electron from HOMO, will mainly take place on the ligands. Furthermore, values of Table 4 also evidence that the levels of HOMO and LUMO of the ligands can be tuned through the nature of substituents and that the coordination to the cluster [Mo₂(V)O₂S₂]²⁺ induces a stabilization of the HOMO in comparison with the uncoordinated ligands.

3.7. Biological activity

3.7.1. Antifungal activity

The antifungal activity of [Mo₂(V)O₂S₂]²⁺ complexes with thiosemicarbazone ligands and with “classical” ligands L-histidine, L-cysteine, nitrilotriacetate, and EDTA against *Cryptococcus neoformans* and *Candida albicans* was recently reported by Fuior et al. [11,34]. With classical ligands, no activity was measured against *Candida albicans* [11]. On the contrary, when thiosemicarbazone complexes are tested, the activity of complexes against *Candida albicans* with ligands possessing a pyridine ring as R¹ group show interesting values of MIC in the range 3.9–7.8 μg/mL, while the ligand bearing quinoline, phenol, thiophen and furan derivatives are not or poorly active [34]. The complexes with classical ligands remain not or poorly active against *Cryptococcus neoformans*, while the thiosemicarbazone complexes tested by Fuior et al. appear highly efficient on *Cryptococcus neoformans* (MIC in the range 0.49–31.25 μg/mL), whatever the nature of the thiosemicarbazone ligand [34]. These results suggest that the ligand should play a crucial role for the antifungal activity of the Mo₂O₂S₂-based complexes.

To bring more element for understanding this behaviour, we investigated the 5 ligands alone and the corresponding complexes formed with [Mo₂(V)O₂S₂]²⁺. The results are gathered in Table 6 in comparison with some selected previous results of Fuior et al. [11,34] (for clarity, ligands from previous study are drawn in Scheme 3).



Scheme 3. Structures of the ligands used in a previous study [34].

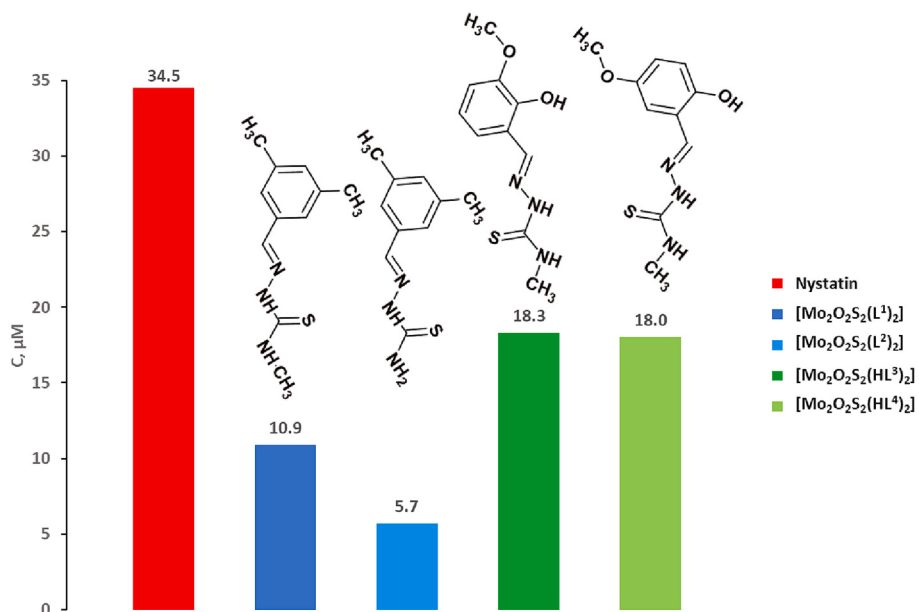


Fig. 7. Antifungal activity of complexes $[Mo_2O_2S_2(H_nL^{1-4})_2]$, $n = 0-1$ against *Cryptococcus neoformans*.

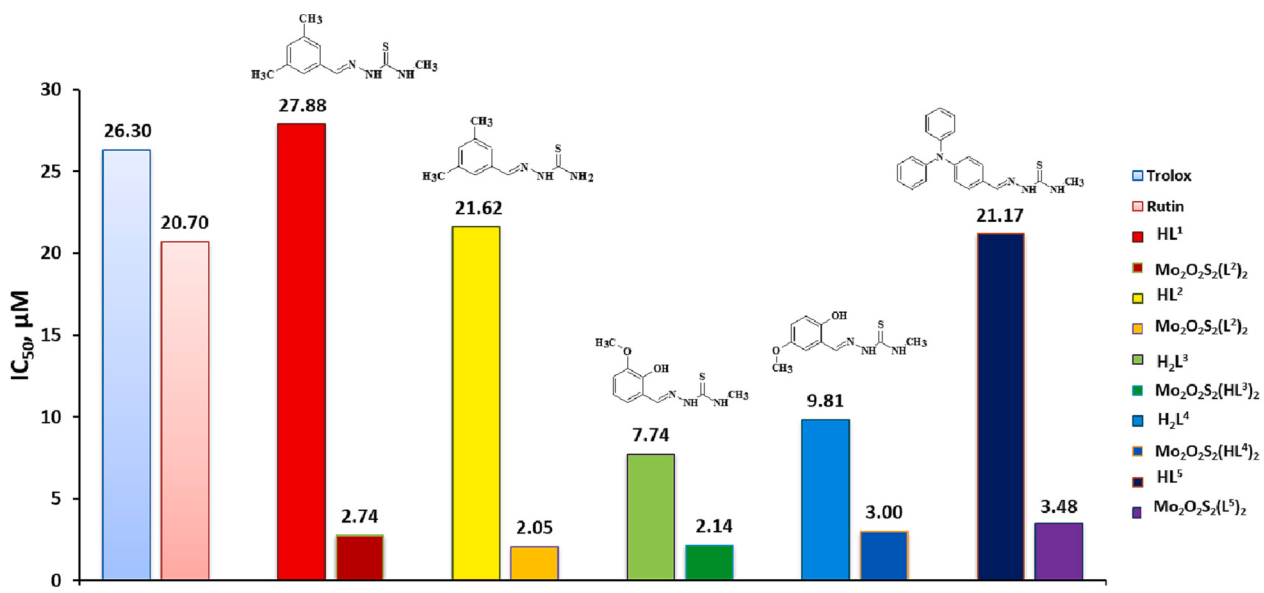


Fig. 8. Antioxidant activities (ABTS) for complexes $[Mo_2O_2S_2(H_nL^{1-5})_2]$, $n = 0-1$ and ligands in comparison with TROLOX and RUTIN references.

Interestingly, the non-coordinated thiosemicarbazone ligands HL^5 are all inactive against both *Cryptococcus neoformans* and *Candida albicans*. Similarly, the complexes $[Mo_2O_2S_2(L^1)_2]$, $[Mo_2O_2S_2(L^2)_2]$, $[Mo_2O_2S_2(HL^3)_2]$, $[Mo_2O_2S_2(HL^4)_2]$ and $[Mo_2O_2S_2(HL^5)_2]$ are also inactive on *Candida albicans*.

Conversely, the activity of complexes $[Mo_2O_2S_2(L^1)_2]$, $[Mo_2O_2S_2(L^2)_2]$, $[Mo_2O_2S_2(HL^3)_2]$, and $[Mo_2O_2S_2(HL^4)_2]$ (or complexes resulting from the partial degradation of the initial complexes) on *Cryptococcus neoformans* is higher than the reference compound Nystatin (see Fig. 7 and Table 5) and of the same order than the $Mo_2O_2S_2$ -based thiosemicarbazone complexes previously reported [34]. However, the last complex $[Mo_2O_2S_2(HL^5)_2]$ appears inactive. These results demonstrate i) that the activity of the $Mo_2O_2S_2$ -based thiosemicarbazone complexes are probably due to the coordinated ligands, ii) that the association of certain thiosemicarbazone ligands with the $[Mo_2O_2S_2]^{2+}$ cluster probably leads to additive effect of both moieties and thus to

systems that are highly active against *Cryptococcus neoformans* and iii) that the activity of the complexes can be partially tuned through the choice of the group R^1 on the ligand but the activity is not lost when R^1 is a non-coordinative group. Moreover, when comparing the complexes $[Mo_2O_2S_2(L^1)_2]$ and $[Mo_2O_2S_2(L^2)_2]$, it is found that the complex with -NH₂ is more active than its counterpart with NH-CH₃. In the case of complexes $[Mo_2O_2S_2(HL^3)_2]$ and $[Mo_2O_2S_2(HL^4)_2]$, it was found that the position of the -OCH₃ group does not influence the antifungal activity.

Finally, these studies performed against *Candida albicans* and *Cryptococcus neoformans* evidence a selective fungicidal activity of the $Mo_2O_2S_2$ -based thiosemicarbazone complexes of this study against fungi of the species *Cryptococcus neoformans*.

3.7.2. Antioxidative properties

Free radicals are involved in many major physiological processes in

Table 7
Antioxidant activities for ligands and $\text{Mo}_2\text{O}_2\text{S}_2$ complexes against ABTS.

| Compounds | IC_{50} (μM) | TEAC ^a |
|---|------------------------------------|-------------------|
| HL^1 | 27.88 ± 0.35 | 0.94 |
| HL^2 | 21.62 ± 0.39 | 1.22 |
| H_2L^3 | 7.74 ± 0.05 | 3.40 |
| H_2L^4 | 9.81 ± 0.03 | 2.68 |
| HL^5 | 21.17 ± 0.42 | 1.24 |
| L-histidine [11] | >100 | — |
| L-cysteine [11] | 28.9 ± 1.0 | 0.91 |
| $[\text{Mo}_2\text{O}_2\text{S}_2(\text{L}^1)_2]$ | 2.74 ± 0.04 | 9.60 |
| $[\text{Mo}_2\text{O}_2\text{S}_2(\text{L}^2)_2]$ | 2.05 ± 0.36 | 12.83 |
| $[\text{Mo}_2\text{O}_2\text{S}_2(\text{L}^3)_2]$ | 2.14 ± 0.05 | 12.29 |
| $[\text{Mo}_2\text{O}_2\text{S}_2(\text{L}^4)_2]$ | 3.00 ± 0.89 | 8.77 |
| $[\text{Mo}_2\text{O}_2\text{S}_2(\text{L}^5)_2]$ | 3.48 ± 0.66 | 7.56 |
| $[\text{Mo}_2\text{O}_2\text{S}_2(\text{Lhis})_2]$ [11] | 7.00 ± 0.40 | 3.76 |
| $\text{K}_2[\text{Mo}_2\text{O}_2\text{S}_2(\text{Lcys})_2]$ [11] | 1.9 ± 0.2 | 13.84 |
| Trolox | 26.30 ± 0.70 | 1 |
| Rutin | 20.70 ± 0.12 | 1.27 |

^a TEAC = ratio of the activity Trolox on the activity of a compound X; TEAC = 1 means similar activity; TEAC > 1 means “more active than Trolox”; TEAC < 1 means “less active than Trolox”.

living organisms, causing aging of living beings and development of various diseases. Therefore, antioxidants have the potential to protect cells, tissues and prevent aging of the body. According to previous studies, the molybdenum fragment $[\text{Mo}_2\text{O}_2\text{S}_2]^{2+}$ is known as an active redox centre, and Mo(V) atoms can be oxidized to Mo(VI) [5,51,52]. Besides, previous studies by Fuior et al. reported interesting antioxidant properties of $[\text{Mo}^{(\text{V})}_2\text{O}_2\text{S}_2]^{2+}$ -based complexes, especially with L-histidine and L-cysteine ligands, while complexes with ligands such as EDTA or HNTA and $[\text{Mo}^{(\text{V})}_2\text{O}_4]^{2+}$ -based complexes were inactive [11], thus suggesting that this process could be localized on the $[\text{Mo}^{(\text{V})}_2\text{O}_2\text{S}_2]^{2+}$ cluster. To our knowledge there is no data reported so far in the literature about other Mo(V) complexes. However, Eglen-Bakir et al. reported some series of complexes of general formula $[\text{Mo}^{(\text{V})}_2\text{O}_2(\text{L})(\text{solvent})]$ where L is a tridentate thiosemicarbazone (ONN or ONS) ligand [26,53–55]. They evidenced not only antioxidant properties of ligands alone but also antioxidant capacities for the corresponding complexes with $[\text{Mo}^{(\text{V})}\text{O}_2]^{2+}$ moiety. For these complexes, the activity is necessarily localized on the ligand and the antioxidant capacity of ligands and complexes are usually comparable to the reference compound TROLOX. But the activity clearly depends on the method used (ABTS or DPPH), the nature of the ligands and substituents in the ligands, the coordination mode of the ligands, the solvent, and the presence or not of protons in the ligands and/or complexes. In some series, the complexes have a lower IC_{50} than ligands [54,55], while the opposite is true in other series [26,53].

In this study, we measured the antioxidant activity by the ABTS method for ligands and complexes in comparison with the reference compounds TROLOX and RUTIN. The results are gathered in Fig. 8 and in Table 7.

The five thiosemicarbazone ligands in this study show comparable or superior antioxidant capacity to TROLOX. In particular, the two ligands H_2L^3 and H_2L^4 bearing phenolic groups were found to be the best candidates among the five ligands. Comparison between HL^1 and HL^2 , which differ only by one methyl group on the terminal amine function, shows slightly higher activity for HL^2 with the terminal -NH₂ group compared to HL^1 with the terminal -NHMe group. This may suggest that protons have a beneficial effect, as observed in the tests with DPPH radicals, but not with ABTS to our knowledge [55].

Interestingly, the complexes formed with the $[\text{Mo}^{(\text{V})}_2\text{O}_2\text{S}_2]^{2+}$ cluster appear to be much more active against ABTS with an IC_{50} in the range 2.05–3.48 μM , which translates to a TEAC (Trolox Equivalent Antioxidant Capacity, TEAC > 1 means “more active than Trolox”) in the range 7.56–12.83. These results are similar to the data obtained with L-cysteine ligand, i.e., $\text{IC}_{50} = 28.9 \mu\text{M}$, and its corresponding complex

$[\text{Mo}_2^{(\text{V})}\text{O}_2\text{S}_2(\text{LCys})_2]^{2-}$ with $\text{IC}_{50} = 1.9 \mu\text{M}$ (TEAC = 13.84) [11] and are also in agreement with previous study of Fuior et al. in which the activity of ligand was only partially reported [34].

In contrast to the studies of Eglen-Bakir et al. on Mo(+VI)-thiosemicarbazone complexes, both the ligands and the $[\text{Mo}^{(\text{V})}_2\text{O}_2\text{S}_2]^{2+}$ cluster can be active in our complexes due to the lower oxidation state of the metal centre. Nevertheless, DFT calculation evidences that i) the HOMO orbitals are mainly centred on the ligands in the complexes, and ii) the HOMO-LUMO gap systematically decreases from ligands to the complexes (see Table 4). Therefore, the redox process is most likely centred on the thiosemicarbazone ligands and coordination with $[\text{Mo}^{(\text{V})}_2\text{O}_2\text{S}_2]^{2+}$ results in a perturbation of the energy levels that exalt the activity of the ligands. It must be also the case of the previously reported complex $[\text{Mo}^{(\text{V})}_2\text{O}_2\text{S}_2(\text{LCys})_2]^{2-}$ in which the L-cysteine ligand is also probably the centre of the antioxidative activity of the complex [11].

4. Conclusions

In this study, we synthesized five new complexes associating novel thiosemicarbazone ligands to the cluster $[\text{Mo}_2\text{O}_2\text{S}_2]^{2+}$. The complexes were characterized in the solid state and in solution by various analytical techniques including X-ray diffraction, MALDI-TOF mass spectrometry, and NMR spectroscopy. The results showed the formation of mixture of isomers in solution, consisting mainly of *trans* and *cis* configurations in complexes of 1:2 (metal cluster:ligand) stoichiometry. DFT calculations revealed that, in most of the cases, the *cis* configuration is favoured due to the stabilizing effect of π - π stacking of the aromatic moieties present in the ligands. Therefore, to address the issue of mixture of isomers, other synthetic strategies must be developed, such as the use of bis-thiosemicarbazone ligands. This work is currently in progress.

The antifungal and the antioxidative activities of ligands and complexes were studied. Selective fungicidal activity against fungus *Cryptococcus neoformans* CECT 1043 was observed for all complexes, while the ligands alone were inactive. Finally, the antioxidative capacity of ligands and complexes was evaluated on ABTS radicals. High activity was measured for the ligands alone and this activity was even stronger when these ligands are complexed with the cluster $[\text{Mo}_2\text{O}_2\text{S}_2]^{2+}$. DFT calculations confirmed that the redox process is most likely takes place on the ligands, and that complex formation significantly reduces the HOMO-LUMO gap, further facilitating electron transfer.

Author statement

Diana Cebotari: synthesis of ligands and complexes,
Olga Garbuz, Greta Balan : biological tests

Mohamed Haouas : NMR studies

Aurelian Gulea: coordination of the biological tests.

Jérôme Marrot : X-Ray diffraction studies

Vincent Guérineau, David Touboul: MALDI-TOF studies

Jordi Buils, Mireia Segado Centellas, Carles Bo: DFT studies

Sébastien Floquet : supervisor of this study

Declaration of Competing Interest

The authors declare that they have no known competing financial interests or personal relationships that could have appeared to influence the work reported in this paper.

Data availability

Data will be made available on request.

Acknowledgements

University of Versailles, the “Institut Universitaire de France, IUF”

and the CNRS are gratefully acknowledged for financial support. DC gratefully acknowledge Campus France for Excellence Eiffel grants as well as State University of Moldova for funding her PhD thesis. This work is supported by the “ADI 2019” project funded by the IDEX Paris-Saclay, ANR-11-IDEX-0003-02, “Joint research projects AUF-MECR 2020-2021” funding program, and National Agency for Research and Development (ANCD) of the Republic of Moldova (Project No 20.80009.5007.10 and Project No 20.80009.7007.12), which are gratefully acknowledged. The authors thank the ICIQ Foundation, CERCA Program of the Generalitat de Catalunya, and the Spanish Ministerio de Ciencia e Innovacion through projects PID2020-112806RB-I00 and the Severo Ochoa Excellence Accreditation 2020–2023 CEX2019-000925-S. This study results from an International collaboration supported by IRN-CNRS 2019-2023.

Appendix A. Supplementary data

The Supporting Information contains, FT-IR spectra (Fig. S1); ESI-MS spectra of ligands (Figs. S2-S6); experimental and simulated MALDI-TOF spectra of complexes not shown in the main text (Figs. S7-S10); a view of interaction between complex and DMSO within the structure of complex $[\text{Mo}_2\text{O}_2\text{S}_2(\text{HL}^3)_2]$ (Fig. S11); a summary of NMR data for ligands and complexes (Tables S1-S2); ^{13}C NMR spectra of ligands (Figs. S12-S16); deconvoluted ^1H NMR spectra of complexes at 10^{-2} M not shown in the main text (Figs. S17-S20); NMR spectra of $[\text{Mo}_2\text{O}_2\text{S}_2(\text{L}^1)_2]$ at different concentration (Fig. S21); Evolution of the ^1H NMR spectra of complexes at 5 mM during 72 h (Figs. S22-S26); pictures of structures optimized by DFT and HOMO and LUMO orbitals for ligands and complexes (Figs. S27-S28, Table S3). Supplementary data to this article can be found online at [<https://doi.org/10.1016/j.jinorgbio.2023.112258>].

References

- [1] R. Hille, Trends Biochem. Sci. 27 (2002) 360.
- [2] R. Hille, T. Nishino, F. Bittner, Coord. Chem. Rev. 255 (2011) 1179.
- [3] R. Hille, R. Mendel, Coord. Chem. Rev. 255 (2011) 991.
- [4] B. Spivack, Z. Dori, J. Chem. Soc. Chem. Commun. (1970) 1716.
- [5] V.R. Ott, D.S. Swieter, F.A. Schultz, Inorg. Chem. 16 (1977) 2538.
- [6] B. Spivack, Z. Dori, Coord. Chem. Rev. 17 (1975) 99.
- [7] J. Gretarsdottir, I. Lambert, S. Sturup, S. Suman, ACS Pharmacol. Transl. Sci. 5 (2022) 907.
- [8] S.G. Suman, J.M. Gretarsdottir, P.E. Penwell, J.P. Gunnarsson, S. Frostason, S. Jonsdottir, K.K. Damodaran, A. Hirschon, Inorg. Chem. 59 (2020) 7644.
- [9] S.G. Suman, J.M. Gretarsdottir, T. Snaebjornsson, G.R. Runarsdottir, P.E. Penwell, S. Brill, C. Green, J. Biol. Inorg. Chem. 19 (2014) S760.
- [10] J.M. Gretarsdottir, S. Jonsdottir, W. Lewis, T.W. Hambley, S.G. Suman, Inorg. Chem. 59 (2020) 18190.
- [11] A. Fuior, A. Hijazi, O. Garbuz, V. Bulimaga, L. Zosim, D. Cebotari, M. Haouas, I. Toderas, A. Gulea, S. Floquet, J. Inorg. Biochem. (2022) 226.
- [12] J.S. Casas, M.S. Garcia-Tasende, J. Sordo, Coord. Chem. Rev. 209 (2000) 197.
- [13] T.S. Lobana, R. Sharma, G. Bawa, S. Khanna, Coord. Chem. Rev. 253 (2009) 977.
- [14] E. Pahontu, I. Usataia, V. Graur, Y. Chumakov, P. Petrenko, V. Gudumac, A. Gulea, Appl. Organomet. Chem. 32 (2018), e4544.
- [15] R.B. Singh, H. Ishii, Crit. Rev. Anal. Chem. 22 (1991) 381.
- [16] L.N. Suvarapu, A.R. Somala, J.R. Koduru, S.O. Baek, V.R. Ammireddy, Asian J. Chem. 24 (2012) 1889.
- [17] K.L. Summers, Mini-Rev. Med. Chem. 19 (2019) 569.
- [18] Z.-G. Jiang, M.S. Lebowitz, H.A. Ghanbari, Cns Drug Rev. 12 (2006) 77.
- [19] H. Beraldo, D. Gambino, Mini-Rev. Med. Chem. 4 (2004) 31.
- [20] B. Shakya, P.N. Yadav, Mini-Rev. Med. Chem. 20 (2020) 638.
- [21] E. Pahontu, M. Proks, S. Shova, G. Lupascu, D.-C. Ilies, S.-F. Barbuceanu, L.-I. Socea, M. Badea, V. Paunescu, D. Istrati, A. Gulea, D. Dragomescu, C.E.D. Pirvu, Appl. Organomet. Chem. 33 (2019), e5185.
- [22] E. Pahontu, D.-C. Ilies, S. Shova, C. Orcean, V. Paunescu, O.T. Olaru, F. S. Radulescu, A. Gulea, T. Rosu, D. Dragomescu, Molecules 22 (2017) 650.
- [23] T. Rosu, E. Pahontu, S. Pascalescu, R. Georgescu, N. Stanica, A. Curaj, A. Popescu, M. Leabu, Eur. J. Med. Chem. 45 (2010) 1627.
- [24] G. Balan, O. Burduinic, I. Usataia, V. Graur, Y. Chumakov, P. Petrenko, V. Gudumac, A. Gulea, E. Pahontu, Appl. Organomet. Chem. 34 (2020), e5423.
- [25] H.A. El-Ghamry, M. Gaber, T.A. Farghaly, Mini-Rev. Med. Chem. 19 (2019) 1068.
- [26] S. Eglence-Baker, O. Sacan, M. Sahin, R. Yanardag, B. Ulkuseven, J. Mol. Struct. 1194 (2019) 35.
- [27] V. Vrdoljak, I. Dilović, M. Rubčić, S. Kraljević Pavelić, M. Kralj, D. Matković-Čalogović, I. Piantanida, P. Novak, A. Rožman, M. Cindrić, Eur. J. Med. Chem. 45 (2010) 38.
- [28] S. Celen, S. Eglence-Bakir, M. Sahin, I. Deniz, H. Celik, I. Kizilcikli, J. Coord. Chem. 72 (2019) 1747.
- [29] J. Pisk, B. Prugovecki, D. Matkovic-Calogovic, R. Poli, D. Agustin, V. Vrdoljak, Polyhedron 33 (2012) 441.
- [30] V. Vrdoljak, D. Milic, M. Cindric, D. Matkovic-Calogovic, J. Pisk, M. Markovic, P. Novak, Z. Anorg. Allg. Chem. 635 (2009) 1242.
- [31] V. Vrdoljak, J. Pisk, B. Prugovecki, D. Matkovic-Calogovic, Inorg. Chim. Acta 362 (2009) 4059.
- [32] V. Vrdoljak, D. Milic, M. Cindric, D. Matkovic-Calogovic, D. Cincic, Polyhedron 26 (2007) 3363.
- [33] A. Fuior, D. Cebotari, M. Haouas, J. Marrot, G. Espallargas, V. Guerineau, D. Touboul, R. Rusnac, A. Gulea, S. Floquet, ACS Omega 7 (2022) 16547.
- [34] A. Fuior, D. Cebotari, O. Garbuz, S. Calancea, A. Gulea, S. Floquet, Inorg. Chim. Acta 548 (2023), 121372.
- [35] G. M. Sheldrick, 1999.
- [36] G.M. Sheldrick, Acta Crystallogr. Sect. C Struct. Chem. 71 (2015) 3.
- [37] C.B. Hübschle, G.M. Sheldrick, B. Dittrich, J. Appl. Crystallogr. 44 (2011) 1281.
- [38] G. te Velde, F. Bickelhaupt, E. Baerends, C. Guerra, S. Van Gisbergen, J. Snijders, T. Ziegler, J. Comput. Chem. 22 (2001) 931.
- [39] A. Becke, Phys. Rev. A 38 (1988) 3098.
- [40] J. Perdew, Phys. Rev. B 33 (1986) 8822.
- [41] S. Grimme, J. Antony, S. Ehrlich, H. Krieg, J. Chem. Phys. (2010) 132.
- [42] E. Vanlenthe, E. Baerends, J. Snijders, J. Chem. Phys. 99 (1993) 4597.
- [43] A. Klamt, J. Phys. Chem. 99 (1995) 2224.
- [44] E. Cadot, B. Salignac, J. Marrot, A. Dolbecq, F. Secheresse, Chem. Commun. (2000) 261.
- [45] E. Pahontu, V. Fala, A. Gulea, D. Poirier, V. Tapcov, T. Rosu, Molecules 18 (2013) 8812.
- [46] J.-F. Lemmonier, S. Duval, S. Floquet, E. Cadot, Isr. J. Chem. 51 (2011) 290.
- [47] E. Cadot, B. Salignac, S. Halut, F. Secheresse, Angew. Chem. Int. Ed. 37 (1998) 611.
- [48] A. Hijazi, J.C. Kemmegne-Mbouguen, S. Floquet, J. Marrot, J. Fize, V. Artero, O. David, E. Magnier, B. Pegot, E. Cadot, Dalton Trans. 42 (2013) 4848.
- [49] A. Hijazi, J.C. Kemmegne-Mbouguen, S. Floquet, J. Marrot, C.R. Mayer, V. Artero, E. Cadot, Inorg. Chem. 50 (2011) 9031.
- [50] V. Vrdoljak, M. Cindric, D. Milic, D. Matkovic-Calogovic, P. Novak, B. Kamenar, Polyhedron 24 (2005) 1717.
- [51] J.C. Kemmegne-Mbouguen, S. Floquet, D. Zang, A. Bonnefont, L. Ruhlmann, C. Simonnet-Jegat, X. Lopez, M. Haouas, E. Cadot, New J. Chem. 43 (2019) 1146.
- [52] J.C. Kemmegne-Mbouguen, S. Floquet, E. Cadot, Comptes Rendus Chim. 24 (2021) 91.
- [53] S. Eglence, M. Sahin, M. Ozyurek, R. Apak, B. Ulkuseven, Inorg. Chim. Acta 469 (2018) 495.
- [54] S. Eglence-Baker, M. Sahin, M. Zahoor, E. Dilmen-Portakal, B. Ulkuseven, Polyhedron 190 (2020), 114754.
- [55] S. Eglence-Bakir, M. Sahin, M. Ozyurek, B. Ulkuseven, Polyhedron (2021) 209.